Modelling Entrainment of Sedimentary Particles by Wind and Water: A Generalized Approach

Hua Lu[1,a] **, Michael R. Raupach**[b] **and Keith S. Richards**[c]

[1] *British Antarctic Survey, Cambridge, UK*

[a] *The Institute of Theoretical Physics, University of Cambridge, UK*

[b] *CSIRO Marine and Atmospheric Research, Canberra, AUSTRALIA*

[c] *Department of Geography, University of Cambridge, UK*

Abstract: For longstanding theoretical reasons, it is often asserted that the threshold shear stress for entrainment of sedimentary particles ($\tau_{*t} = \rho_f u_{*t}^2$, made dimensionless as $A = \rho_f u_{*t}^2 \big/ \left((\rho_p - \rho_f) g d \right)$), has a universal relationship with the particle Reynolds number ($\mathrm{Re}_{*t} = u_{*t} d / \nu$), where u_{*t} is the threshold friction velocity, ρ_f is the fluid density, ρ_p is the density of the particles, d is the particle diameter, g is the gravitational acceleration and ν is the kinematic viscosity of the fluid. However, experimental plots of $A(\mathrm{Re}_{*t})$ for sediment entrainment in air and water show two major differences: (1) for large Re_{*t}, the values of A in water are, in general, a few times larger than those in air, and (2) when $\mathrm{Re}_{*t} < 1$, A increases more rapidly in air than in water as Re_{*t} decreases. This paper derives a new, general theory for A, which incorporates the effects of fluid turbulence, particle cohesion and probabilistic aspects of grain entrainment. It is found that difference (1) is explained by differences in the probability distribution of streamwise velocity fluctuations for typical situations in air and water, which follow from basic scaling laws for velocity variances in turbulent flow. Difference (2) is explained by the different behaviours of interparticle cohesion forces in air and water. The resulting expression is shown to compare well with experimental data.

Keywords: sediment; entrainment; threshold shear stress; threshold velocity; near-surface turbulent fluctuations.

1. Introduction

The prediction of incipient motion of a particle lying in a bed of similar particles (*i.e.* the entrainment of sedimentary particles from the surface into the fluid when the fluid speed exceeds a certain threshold), is fundamental for understanding sediment transport by water and wind [*Graf*, 1971; *Quan and Wan*, 1983; *Nickling*, 1988; *Raupach and Lu*, 2004]. *Shields* [1936] pioneered research into incipient motion in open channels by introducing the dimensionless threshold shear stress $A = \tau_{*t}/(\rho_p - \rho_f)g\,d$, a measure of the ratio of the threshold hydrodynamic force on a surface particle to its weight (see Table 1 for definitions of symbols). *Shields* argued that A should be a unique function of the particle Reynolds number $\mathrm{Re}_{*t} = u_{*t}\,d/\nu$, as

$$A = F(\mathrm{Re}_{*t})\,. \qquad (1)$$

For particle entrainment by air flow, *Bagnold* [1941] derived a similar theory considering the balance between the aerodynamic drag and the gravitational force. He found that at large Re_{*t}, A is nearly a constant and $u_{*t} \propto d^{1/2}$, which is essentially consistent with *Shields*' theory obtained in open channels. Across all particle sizes, *Bagnold* also assumed that A is a unique function of Re_{*t}, again consistent with the proposals of *Shields*.

Over the last 70 years, experimental research into incipient motion has in general supported the theories of *Shields* and *Bagnold* [*White*, 1970; *Graf*, 1971; *Yalin*, 1972; *Mantz*, 1977; *Buffington and Montgomery*, 1997; *Zingg*, 1953; *Greeley and Iversen*, 1985; *Nickling*, 1988]. Figure 1 shows data obtained in experiments in air [*Cleaver and Yates*, 1973; *Fletcher*, 1976a,b; *Iversen and White*, 1982;] and in water [*Graf*, 1971; *Yalin*, 1972; *White*, 1970], plotted on a typical *Shields*' $A \sim \mathrm{Re}_{*t}$ diagram. Three distinct regions can be identified:

i) $\mathrm{Re}_{*t} \geq 10$; a region where the flow is fully turbulent, and where A attains a constant value of approximately 0.04 to 0.06 at $\mathrm{Re}_{*t} \geq 500$ in water, and 0.01 to 0.03 in air (note that there are few data with $\mathrm{Re}_{*t} \geq 200$ for air flows);

ii) $\mathrm{Re}_{*t} < 1$; a region where particle entrainment is mainly due to viscous laminar flow, where A increases while Re_{*t} decreases, at a rate which is steeper in air than in water; and

iii) A transitional region, $1 \leq \mathrm{Re}_{*t} \leq 10$, where the laminar sublayer partially covers the particles, but the outer turbulent flow is partially affected by the roughness of the grain bed. Within this region, A reaches a minimum value of approximately 0.03 to 0.06 for water [*Yalin and Karahan*, 1979], but such minima are not obvious for air entrainment [*Greeley and Iversen*, 1985].

Figure 1 shows that data obtained from airflow and open channel flow do not collapse to a single $A \sim \mathrm{Re}_{*t}$ relationship. The upturn of the *Shields* curve at $Re_{*t} < 1$ in air flow is much sharper than for water flow. For $Re_{*t} \geq 5$, A is about 3 to 4 times smaller in air than in water.

[[Insert Figure 1 here]]

Several researchers have noted the different behaviour of A in air and in water, and that the expressions for A derived in one fluid cannot be directly applied to another [*Bagnold*, 1941; *Graf*, 1971; *Iversen and Pollack*, 1987]. *Bagnold* [1941] suggested that the differences might be due to a difference in surface texture or bed packing conditions, or to observation errors. *Iversen and Pollack* [1987] attributed the difference to density ratio differences. By adding the impacting force of saltating particles to the force balance equation, they related A empirically to the particle-to-fluid density ratio. Although not directly targeting the different behaviour of A in air and in water, a recent study of incipient motion in air has also incorporated the effect of the particle-to-fluid density ratio [*Cornelis and Gabriels*, 2004]. Interestingly, although *Cornelis and Gabriels* [2004] and *Iversen and Pollack* [1987] both related A to the density ratio, and both utilized the same data of *Iversen and White* [1982], the expression of *Iversen and Pollack* [1987] suggests that A decreases with increasing particle-to-fluid density ratio while the expression of *Cornelis and Gabriels* [2004] suggests A increases with increasing density ratio. Making the situation more confusing, a comprehensive review of incipient motion in open channel flow concludes that there is no obvious dependence of A on particle density, therefore, on density ratio [*Buffington and Montgomery* 1997]. These contradictions suggest that the quantitative relationships between A and flow conditions, fluid properties and particle properties remain unclear. It is also not clear why, for a given fluid and under similar experimental conditions, randomly-varying values of A have often been obtained.

Much research into incipient motion has been based on a force balance at the instant of particle entrainment [*Bagnold*, 1941; *Phillips*, 1980; *Iversen and White*, 1982], and/or analysis of dimensionless groups [*Shields*, 1936; *Fletcher*, 1976a,b]. With certain assumptions, the functional forms for the parameter A are predetermined and then fitted to experimental data, and in some cases, excessive parameter fitting is involved [*Greeley and Iversen*, 1985; *Cornelis and Gabriels*, 2004]. These studies have provided a means of estimating threshold shear stress under idealized situations. Nevertheless, such a deterministic reductionism often results in partial explanations of the several processes involved in incipient motion. Apart from the inability to explain differences of $A \sim \mathrm{Re}_{*t}$ relationships in air and water, there is a lack of agreement about the values of A and the physical causes of why, for $\mathrm{Re}_{*t} \leq 1$, the estimates of A vary by an order of magnitude or more for a given Re_{*t}. Emphasizing the effects of flow, *Bagnold* [1956] argued that A will not exceed 0.4, but values

of A greater than 10 have been found for $d \leq 10$ μm [*White,* 1970; *Cleaver and Yates*, 1973; *Fletcher*, 1976a,b]. By assuming laminar sub-layer flow, *Yalin* [1972] derived $A = 0.1/\mathrm{Re}_{*t}$. With similar assumptions for the flow regime and force balance, *Ling* [1995] suggested that A is inversely proportional to Re_{*t} for rolling grains, and inversely proportional to Re_{*t}^2 for a threshold lift condition. Both studies implied that the increase in A with decreasing Re_{*t} is solely due to the transition in flow regime from turbulent to laminar flow.

For particle entrainment in air flow, *Iversen and White* [1982] attributed the sharp upturn of A for $\mathrm{Re}_{*t} < 1$ to the effects of inter-particle cohesion forces. To account for the effect of cohesion, *Greeley and Iversen* [1985] suggested that A should be of the form

$$A = A_1 F(\mathrm{Re}_{*t}) G(d) \qquad (2)$$

where the dimensionless functions $F(\mathrm{Re}_{*t})$ and $G(d)$ respectively represent the effects of aerodynamic and cohesion forces. Eq. (2) essentially implies that the upturn of A for $\mathrm{Re}_{*t} < 1$ is partially due to the flow condition (through the term $F(\mathrm{Re}_{*t})$) and partially due to inter-particle cohesion (through the term $G(d)$). Though eq. (2) overcomes the shortcomings of the early expression of *Bagnold* [1941] and is effective in describing the behaviour of u_{*t} for the entire particle size range, the expressions proposed by *Greeley and Iversen* [1985] involve the two empirical functions, $F(\mathrm{Re}_{*t})$ and $G(d)$, and are difficult to relate to physical processes.

While earlier theoretical analysis often focused on the effects of flow conditions by relating A to the particle Reynolds number Re_{*t}, more recent empirical or semi-empirical studies have to some degree sought to remove the flow term $F(\mathrm{Re}_{*t})$ in eq. (2), or to replace it by a particle property. For instance, *Marticorena and Bergametti* [1995] simplified the expressions of *Greeley and Iversen* [1985] by expressing Re_{*t} as a function of particle size only. *Shao and Lu* [2000] reanalyzed the wind tunnel data of *Iversen and White* [1982] and suggested that $A = A_N G(d)$, where A_N is a constant of 0.013 and $G(d)$ representing the effects of interparticle cohesion,. More recently, *Cornelis and Gabriels* [2004] expressed A as a function of the particle-to-fluid density ratio, particle diameter and interparticle cohesion. Their expression involves five empirical constants that were determined by fitting to the data of *Iversen and White* [1982] using non-linear regression. Such emphases on sedimentological controls are also abundant in the hydraulic literature. For example, in open channels with mixed bed material particle sizes, studies have commonly expressed A as an inverse empirical function of the ratio of particle size d to the underlying median bed particle size d_{50} [*Komar and Li*, 1988; *Richards*, 1990; *Buffington and Montgomery*, 1997].

A clear advantage of using these semi-empirical expressions of A is their simplicity. If A is not expressed as a function of Re_{*t}, iteration is avoided, since the friction velocity u_{*t} no longer appears on both sides of the expression for u_{*t}. This is particularly appealing for large-scale spatially-distributed applications [*Marticorena and Bergametti*, 1995]. However, the drawback of these expressions is their failure to account fully for the physical processes involved. As noted by *Qian and Wan* [1983], a variety of models could fit the experimental data well as long as the chosen expression has the right shape and contains at least two free parameters to describe the upturn of A for both large and small Re_{*t} ranges. There is little basis for judging the superiority of an expression solely on goodness of statistical fit if the physical meaning of the fitted parameters is not clearly understood. A more general, physically-based approach to the threshold of entrainment is needed.

Realizing that deterministic approaches can only estimate the average values of threshold shear stress but unable to predict the observed variations, some researchers have proposed that particle incipient motion is a stochastic process, *i.e.* there exists a range of threshold shear stresses for a given particle size [*Grass*, 1970; *Gessler*, 1971]. Field and laboratory observations in open channel flow confirm a variability of threshold shear stress attributable to a number of random factors including temporal fluctuation of near bed turbulence, the bed packing condition, and heterogeneities in grain size and shape, etc [*Einstein*, 1950; *Grass*, 1970]. In the hydraulic literature, recent research into incipient motion has focused on finding appropriate probability distributions for instantaneous flow velocity or shear stress [*Cheng and Chiew*, 1998; *Wu and Lin*, 2002], the effects of random bed roughness and picking conditions [*Papanicolaou et al.*, 2001; 2002], or the combined probabilistic nature of turbulent fluctuation and bed grain geometry [*Wu and Chou*, 2003]. Nevertheless, incorporating statistical/stochastic concepts remains rare in the modeling of particle incipient motion during wind erosion.

The objective of this paper is to derive a general expression for A, to explain the differences in $A \sim \mathrm{Re}_{*t}$ plots between air and water. We incorporate the effect of fluid turbulence by utilizing recent advances in understanding of turbulence over rough walls, especially the scaling of velocity fluctuations with bulk Reynolds number (using boundary layer height δ as the length scale rather than particle diameter d). We also consider the probabilistic aspects of grain entrainment by adopting a log-normal distribution for the near-bed instantaneous flow velocity. The new expression also incorporates the influences of interparticle cohesion forces to account for the upturning of A for small values of Re_{*t}. We use the new expression to analyze the effects of both the mean flow and turbulent fluctuations, and the physical causes of the different regions in the *Shields*

diagram, which are shown to depend on changes in the relative magnitude of the appropriate forces. Though no direct curve-fitting is used, our results compare well with available experimental data.

2. Methods and The New Theory

This paper considers a flat surface covered by uniformly-sized erodible particles. The *x*-axis lies in the plane of the bed surface, its direction parallel to the direction of flow, while the *y*-axis is perpendicular to the bed and directed upwards. The height origin ($y = 0$) is taken to be the aerodynamic height origin, defined as the level of effective drag or zero-plane displacement (Figure 2). An overbar denotes a temporal average. A superscript $^+$ with a velocity variable (either its mean or fluctuation) denotes normalization by the friction velocity u_*, as in $u^+ = u/u_*$; a similar superscript with a length variable denotes normalization by the viscous length scale ν/u_*, as in $y^+ = u_* y/\nu$. Also, subscripts *a* and *w* denote the air and water cases, respectively.

[[Insert Figure 2 here]]

2.1 Forces Involved in Particle Entrainment

Analysis of the particle threshold condition begins by defining a force balance on a static grain sitting on the bed surface. A particle resting on the bed (Figure 2) is subjected to forces of drag F_D, lift F_L, specific weight F_G and a net cohesion force F_C. We assume that F_C is approximately equal in magnitude to the cohesion force between two adjacent individual particles, but follows the direction of F_G. The forces other than F_C can be expressed as

$$F_G = \frac{\pi}{6}\left(\rho_p - \rho_f\right) g d^3, \tag{3}$$

$$F_D = C_D \frac{\rho_f S u_\Delta^2}{2}, \tag{4}$$

$$F_L = C_L \frac{\rho_f S u_\Delta^2}{2}, \tag{5}$$

where $u_\Delta = \overline{u} + u'$ is a streamwise *reference* instantaneous velocity at the threshold of grain motion, and other symbols are defined in Table 1. The frontal area *S* is approximately equal to $0.2\pi d^2$ for the packing geometry shown in Figure 2.

Choosing the reference height y_Δ where u_Δ is defined can be difficult. *Wu and Lin* [2002] and *Wu and Chou* [2003] effectively calculated y_Δ by integrating both $\overline{u}$ and *u'* over the frontal area of the about-to-move particle exposed to the flow. Such an approach is difficult to justify in fluid mechanical terms, for several reasons. Firstly, one cannot define the instantaneous velocity at a solid surface as zero, because of the no slip condition. Secondly, at any height within the roughness elements, the velocity field is complex and three-dimensional because fluid has to find its way around the roughness elements. Thirdly, the drag on a surface-mounted roughness element does not satisfy a simple momentum integral constraint equivalent to the relationship for a wake of an obstacle in a free stream [*Batchelor,* 1967; *Raupach*, 1992], because of the absence of a free-stream velocity. Finally, an individual roughness element is exposed to a turbulent flow including not only a mean shear but also strong turbulence with contributions both from the large-scale boundary-layer and also the wakes of other roughness elements.

To handle these complexities, it is usual to define u_Δ as the velocity at a reference height y_Δ, horizontally-averaged over an area large enough to smooth out spatial fluctuations caused by the bed roughness (in practice a horizontal distance of order 10*d*). This quantity is analogous to the free stream velocity for the drag coefficient of a body in a uniform flow. In the case of incipient motion, the logical choice for y_Δ is the mean height of the most exposed roughness elements, *i.e.* $y_\Delta = \beta d$, where β is a constant. For instantaneous velocity, the likely choice for β is between 0.5 and 1.0, since the most exposed elements rest some way above the mean position of all bed elements. The level of effective drag or zero-plane displacement (our height origin y = 0) is approximately 0.5*d* to 0.7*d* above the bed substrate level [*Jackson*, 1981; *Bridge and Bennett*, 1992]. *Cheng and Chiew* [1998] suggested $\beta = 0.6$ for the most stable bed packing situation where particles of identical size rest in an interstice formed by closely-packed bed surface particles. In Section 3.1, the effects of β on the values of *A* will be discussed.

The effects of cohesion forces on incipient motion and the dependence of cohesion forces on particle size are complex and poorly understood [*Zimon*, 1982; *Shao and Lu*, 2000; *Cornelis and Gabriels*, 2004]. Cohesion forces arise from both mutual attraction between solid particles, and interaction between the solid particles and those of the ambient fluid medium. The cohesion force is affected by the combination of molecular forces (including the van der Vaal's forces), Coulomb forces, electrostatic forces, capillary forces, and chemical bonding forces. Although these forces are functions of particle size *d*, their dependences on *d* are different, with molecular forces and electrostatic forces proportional to *d*, Coulomb forces proportional to $1/d^2$, the capillary force

proportional to $d(1-d^{x-1})$, where x is the width of a microscopic water bridge in the contact zone of two particles [*Zimon*, 1982]. For instance, the cohesion forces between two identical spheres can be expressed as

$$F_C = \frac{c_i}{32\pi z_i^2} d \ , \tag{6}$$

where c_i is the cohesion coefficient and z_i is the smallest separation between two spherical particles [*Theodoor and Overbeek*, 1985]. Eq. (6) indicates two possible relationships between F_C and d: if z_i is proportional to d, Eq (6) gives F_C proportional to $1/d$ (assuming no dependence of c_i on d), while if z_i is a constant, F_C is proportional to d.

Observations in air have resulted in various relationships between F_C and d: direct, inverse and exponential dependence of the cohesion force on d, or even complete independence over a certain range of d [*Zimon*, 1982]. In water, the dependence of cohesion forces on particle size is simpler and most experiments suggest that F_C is proportional to d [C*orn*, 1961; *Zimon*, 1982]. This is because in water, capillary and electrostatic forces do not apply as any charges on the particles will leak away and no capillary bridge develops within the particle contact zone [*Theodoor and Overbeek*, 1985]. This results in the cohesion force in a liquid medium being governed by molecular forces, which implies direct proportionality to d [*Fuks*, 1955]. Nevertheless, in the case of threshold conditions over a loosely-packed bed with a small removal probability of grains (approximately 2%), direct proportionality between F_C and d may hold in both water and air media as

$$F_C = C_C d \ , \tag{7}$$

where C_C is a proportionality constant, according to *Fuks* [1955] and *Zimon* [1982].

At the instant of particle motion, the combined retarding force moments must just balance the combined hydrodynamic driving force moment. Such a condition is expressed as

$$F_D L_D + F_L L_L = F_G L_G + F_C L_C \ , \tag{8}$$

where $L_D = d\cos\theta$, $L_L = d\sin\theta$, $L_G = d\sin\theta$ and $L_C = d\sin\theta$ are the moment arms (about the pivot point P) of F_D, F_L, F_G and F_C (as shown in Figure 2). Following *Wu and Lin* [2003], the pivoting angle θ ranges from 30° when the grain is at its most exposed, to 90° when it is embedded within the surface grain layer.

Combining eqs. (3) to (5) and (7) with eq. (8), the threshold condition can be written as

$$u_\Delta \geq u_t , \tag{9}$$

where

$$u_t = \sqrt{\frac{2L_w}{C_D L_D + C_L L_L} \frac{\pi d^3}{6S} \frac{(\rho_p - \rho_f) g}{\rho_f} \left(1 + \frac{\rho_f}{(\rho_p - \rho_f) g} \frac{6 C_C L_C}{\pi L_w} \frac{1}{d^2} \right)} \tag{10}$$

is the threshold velocity. Eq. (9) simply states that the instantaneous reference velocity u_Δ must exceed u_t for particle detachment to occur. If we assume u_Δ obeys a certain probability distribution, u_t is therefore defined by a point on the velocity probability distribution of u_Δ at the reference height *y* from the bed where u_Δ is defined, and the probability of particle detachment from the bed is $p = \text{Prob}(u_\Delta \geq u_t)$, as shown in Figure 3. The derivation of *A* based on a log-normal distribution of u_Δ for a given probability removal rate *p* is given in Section 2.4.

[[Insert Figure 3 here]]

We turn now to the values of C_D and C_L. Compared with the well-studied situation of an isolated object in a free stream, where the drag coefficient is a function of Reynolds number ($\text{Re}_* = u_* d / \nu$) and is proportional to $1/\text{Re}_*$ for small Re_*, the drag coefficient for a particle resting on a surface is more complex and less well understood [*Fischer et al.*, 2002; *Jiménez*, 2004]. It has been found that the drag coefficient $C_D \approx 0.15 - 0.30$ for a sphere resting on a surface [*Tillman*, 1944], but may be up to 1.25 for two-dimensional span-wise obstacles [*Jiménez*, 2004]. *Chepil* [1958] provided one of the most comprehensive data sets on the lift coefficient C_L in air, and showed that the average ratio of lift to drag is nearly constant at 0.85 for a boundary layer friction Reynolds number of $\text{Re}_\tau \leq$ 5000, where $\text{Re}_\tau = u_* \delta / \nu$ and δ is the height of the boundary layer. Mainly for channel flows, *James* [1990] proposed

$$\frac{C_L}{C_D} = \begin{cases} -0.56 + 0.212 \ln \text{Re}_* & \text{Re}_* < 150 \\ 0.5 & \text{Re}_* \geq 150 \end{cases} . \tag{11}$$

Eq. (11) suggests that C_L could be negative at $\text{Re}_* < 15$. *Marsh et al*. [2004] derived a similar expression to eq. (11) but with $C_L/C_D \approx 0.2$ for $\text{Re}_* > 100$. The data of *Patnaik et al.* [1994] for gravel-bed rivers showed $C_L/C_D \approx 1$, and an apparent decreasing trend of the lift-to-drag ratio with increasing Re_* in the range 4,000 to 60,000. However, this has limited relevance to this study, where we focus on Re_* in the range from 1 to 10,000. This is because aeolian transport involves a narrower range of particle sizes than in rivers, and in air, there is little reliable data on threshold velocities for $\text{Re}_{*t} > 100$. Furthermore, the exact values for temporally-averaged drag and lift

coefficients are unknown at present, as they both depend upon flow conditions. Though the dependence of C_D and C_L on Re_* is likely to have some effects on A, especially for small Re_*, for simplicity, values of $C_D = 0.5$ and $C_L = 0.3$ are used in this study. According to *Coleman* [1967], for a 3D sphere and $\theta = 30°$, $L_D = d\sqrt{3}/2$, and $L_L = L_G = L_C = d/2$. These values are used here.

2.2 Mean Velocity Profile over Rough Surfaces

The classic theory of near-wall turbulent flow defines the universal logarithmic velocity profile for a smooth wall,

$$\overline{u}^+ = \frac{1}{\kappa}\ln y^+ + B\,, \tag{12}$$

where $\overline{u}$ is the mean flow velocity at height y, κ is von Karman's constant (0.41), and B is an empirical constant with a value of 5.0 [*Clauser*, 1956; *Panton*, 2005]. The effect of roughness on the logarithmic velocity profile is a downward shift of eq. (12), corresponding to the increase in skin friction [*Raupach et al*., 1991]. The logarithmic law for a rough surface can then be written as

$$\overline{u}^+ = \frac{1}{\kappa}\ln y^+ + B - \Delta\overline{u}^+\,. \tag{13}$$

There are three regimes in turbulent flow: smooth, transitionally-rough and fully-rough flow [*Raupach et al*., 1991]. *Ligrani and Moffat* [1986] suggested that these three flow regimes can be classified by $k_s^+ < 2.25$ when the flow is smooth, and $k_s^+ > 90$ when it is fully rough, where $k_s^+ = u_* k_s/\nu$ is the roughness Reynolds number, and k_s is the equivalent sand grain roughness.

The roughness function $\Delta\overline{u}^+$ in eq. (13) has been measured experimentally by *Nikuradse* [1933] using sand roughness of different grain sizes, and in many other experiments over other kinds of rough surface; see Raupach *et al.* [1991] for review. For a uniform sand bed, k_s is equal to the diameter of the particles. *Ligrani and Moffat* [1986] used *Nikuradse's* data to obtain

$$\Delta\overline{u}^+ = \xi\left(\frac{1}{\kappa}\ln k_s^+ + B - 8.5\right), \tag{14}$$

in which the interpolation function

$$\xi = \begin{cases} 0 & k_s^+ < 2.25 \\ \sin\left[\dfrac{\pi\ln\left(k_s^+/2.25\right)}{2\ln\left(90/2.25\right)}\right] & 2.25 \le k_s^+ < 90 \\ 1 & k_s^+ \ge 90 \end{cases} \tag{15}$$

increases from 0 to 1 through the transitionally-rough regime, $2.25 \le k_s^+ < 90$. Eq. (14) recovers the smooth wall log-law in the smooth regime, and suggests that, in the transitionally-rough regime, the roughness function $\Delta\overline{u}^+$ is near zero for k_s^+ below approximately 5.

We note in passing that the rough wall law, eq. (13), is commonly represented as

$$\overline{u}^+ = \frac{1}{\kappa}\ln\left(\frac{y}{z_0}\right), \tag{16}$$

where z_0 is the zero-velocity level of the logarithmic profile. The dimensionless quantities z_0/k_s, ξ and $\Delta\overline{u}^+$ carry equivalent information [*Raupach et al.*, 1991]. Substituting eqs. (13) and (14) into eq. (16) and solving for z_0, we have

$$\begin{aligned} z_0 &= k_s \exp\left[-\ln k^+ - \kappa\left(B - \Delta\overline{u}^+\right)\right] \\ &= k_s \exp\left[\left(\xi - 1\right)\ln k_s^+ + \left(\xi - 1\right)\kappa B - 8.5\kappa\xi\right] \end{aligned}. \tag{17}$$

For fully rough flows, $\xi = 1$ (eq. (15)). Substituting it into eqs. (13) and (17) gives

$$\overline{u}^+ = \frac{1}{\kappa}\ln\left(\frac{y}{k_s}\right) + 8.5, \tag{18}$$

and

$$z_0 / k_s = \exp\left(-8.5\kappa\right) = 0.031, \tag{19}$$

respectively. Eqs. (18) and (19) are consistent with common assumptions in the hydraulics literature and the '$z_0 \sim d/30$ rule' that is commonly known to wind tunnel experimentalists (assuming $d = k_s$ for well sorted sand). In terms of threshold entrainment, all three flow regimes are relevant, depending on particle size and flow conditions. In this study, we shall compare the dimensionless shear stress A resulting from eqs. (13) and (14) with those derived from the fully-rough limit, eqs. (16) and (19).

Some researchers argue that $\overline{u}^+$ depends not only on y^+ but also on the flow Reynolds number [*Barenblatt and Chorin*, 1998]. However, in comparison to that of roughness, such effects are relatively minor in the inner part of the mean velocity profile [*Panton*, 2005] and are not fully understood when roughness elements are present [*Bergstrom et al.*, 2001].

2.3 Reynolds-Number Dependence of Near-bed Turbulent Velocity

Like the mean velocity profile, the turbulence in air and in water is governed by universal dimensionless scaling laws. However, a major distinction between turbulent airflow and turbulent river flow lies in the flow Reynolds number ($\mathrm{Re}_\tau = u_*\delta/\nu$, where δ is the boundary layer depth). Under the conditions of incipient motion, the difference is mainly due to the intrinsic length scale δ, as the difference in viscous length scale u_*/ν of the two media is relatively small. At the threshold condition, the boundary layer depth in a typical wind tunnel is of the order of 1 metre or more [*Greeley and Iversen*, 1985], whereas it is of the order of a few centimetres in laboratory flumes [*Graf*, 1971; *Yalin*, 1972]. The Reynolds number in the atmospheric boundary layer is about 100-1000 times higher than that observed in natural rivers, whereas the sub-layer thickness remains nearly identical [*Metzger and Klewicki*, 2001]. We shall show that these differences are one of the reasons for the systematically smaller values of the dimensionless shear stress A observed in air relative to water (Figure 1).

[[Insert Figure 4 here]]

The turbulent velocity (here considered to be the standard deviation of the streamwise velocity, $\sigma = \sqrt{\overline{u'^2}}$) is a strong function of the Reynolds number [*DeGraaff and Eaton*, 2000; *Metzger and Klewicki*, 2001; *Marusic and Kunkel*, 2003]. As shown in Figure 4, there is a clear dependence of $\sigma^+ = \sigma/u_*$ on the flow Reynolds number Re_τ across all values of the inner variable y^+. *Marusic and Kunkel* [2003] proposed a scaling formulation to account for the full range of turbulence intensity σ^+ in relation to y^+ and Re_τ, based upon the attached eddy hypothesis and the idea that the attached eddy motions in the log region and beyond impose a forcing on the viscous buffer zone and sublayer:

$$(\sigma^+)^2 = \frac{\sigma^2}{u_*^2} = \begin{cases} \dfrac{0.16(y^+)^2}{\left(1+b_1(y^+)^2\right)^{1/2}\left(1+(b_2 y^+)^{2b_3}\right)^{1/2}}\left[1+(\alpha-1)\dfrac{\ln y^+}{\ln 50}\right] & y^+ \le 30 \\ B_1 - B_2\ln\left(\dfrac{y^+}{\mathrm{Re}_\tau}\right) - B_3\left[1-\left(y^+\right)^{-0.9}\right]\left(y^+\right)^{-0.5} & y^+ \ge 150 \end{cases}, \qquad (20)$$

where $\alpha = \dfrac{B_1 - B_2\ln\left(50/\mathrm{Re}_\tau\right)}{B_1 - B_2\ln\left(50/2000\right)}$, $b_1 = 0.008$, $b_2 = 0.115$, $b_3 = 1.6$, $B_1 = 2.39$, $B_2 = 1.03$, and $B_3 = 5.58$. For $30 \le y^+ \le 150$, interpolation is needed. For simplicity, linear interpolation is used in this study. In essence, Eq. (20) describes the behaviour of σ^+ shown in Figure 4, *i.e.* σ^+ increases with

Re_τ and peaks at $y^+ \approx 15$ for a given value of Re_τ. This maximum value of σ^+ can also be expressed as a function of Re_τ

$$\sigma^+_{\max} = \sqrt{0.964 + 0.87 \ln\left(\mathrm{Re}_\tau\right)}\,. \tag{21}$$

The $\sigma^+_{\max} \sim \mathrm{Re}_\tau$ relationship described by eq. (21) is plotted in Figure 5. Typical value ranges of Re_τ for flumes, natural rivers, wind tunnels and atmospheric boundary layers are also shown. This shows that $\sigma^+_{\max} \approx 2.5$ for open channel flow (assuming d = 1 mm, δ = 0.015 m and u_{*t} = 0.03 m s^{-1}), and $\sigma^+_{\max} \approx 3.5$ for air flow in a wind tunnel (assuming d = 1 mm, δ = 1.2 m and u_{*t} = 0.5 m s^{-1}). The former value of $\sigma^+_{\max}$ is consistent with those commonly used in the hydraulic literature [*Cheng and Chiew*, 1998; *Wu and Lin*, 2002].

[[Insert Figure 5 here]]

Though eqs. (20) and (21) were developed for smooth surfaces, recent studies show that roughness enhances the turbulence and the Reynolds shear stress over most of the boundary layer, and promotes isotropy as a result of mixing caused by the wakes generated by the roughness elements [*Raupach et al.* 1996; *Krogstad and Antonia*, 1999; *Tachie et al*., 2004]. However, for a sand surface, the increment of turbulence intensity is quite small for the streamwise component [*Tachie at al.*, 2004], in contrast with surfaces of higher roughness such as vegetation. Therefore, eqs. (20) and (21) are used in our analysis.

2.4 Entrainment Probability in a Log-Normal Distribution of Instantaneous Velocities

The near-bed turbulence is intense and dominated by gust-like eddy motions with length scales determined by the characteristic length scale of the roughness, k_s or d [*Raupach et al.* 1991, 1996]. These gusts cause the streamwise velocity to show significant departure from a normal velocity distribution [*Morrison et al.*, 2004], with strong positive skewness near the bed. It is reasonable to describe the highly positively skewed distribution for the instantaneous velocity u_Δ as log-normal [*Wu and Lin*, 2002] (Figure 3). Thus, we assume that if υ_Δ denotes the logarithm of u_Δ (*i.e.* $\upsilon_\Delta = \ln u_\Delta$), the probability density function $f\left(\upsilon_\Delta\right)$ obeys a normal distribution:

$$f_\upsilon(\upsilon_\Delta) = \frac{1}{\sqrt{2\pi\sigma_\upsilon}} \exp\left[-\frac{\left(\upsilon_\Delta - \overline{\upsilon_\Delta}\right)^2}{2\sigma_\upsilon^2}\right] \tag{22}$$

where $\overline{\upsilon_\Delta}$ and σ_υ are the mean and standard deviation of υ_Δ, respectively.

The probability of entrainment (p) can be expressed as

$$p = \text{Prob}\left(u_\Delta \geq u_t\right) = \text{Prob}\left(\upsilon_\Delta \geq \upsilon_t\right) = 1 - \text{Prob}\left(-\infty < \upsilon_\Delta < \upsilon_t\right) \tag{23}$$

where $\upsilon_t = \ln u_t$ and u_t is the threshold velocity determined by eq. (10). Physically, p can be interpreted as the fraction of the time over which the instantaneous reference velocity u_Δ must exceed the threshold velocity u_t for detachment to occur. As will be shown later, p emerges as a critical parameter in estimating A. Using an approximation for the error function [*Cheng and Chiew*, 1998], we have

$$p = 1 - \left[\int_{-\infty}^{\overline{\upsilon_\Delta}} f_\upsilon\left(\upsilon_\Delta\right)\mathrm{d}\upsilon_\Delta + \int_{\overline{\upsilon_\Delta}}^{\upsilon_t} f_\upsilon\left(\upsilon_\Delta\right)\mathrm{d}\upsilon_\Delta\right]$$
$$0.5\left(1 - \frac{\upsilon_t - \overline{\upsilon_\Delta}}{\left|\upsilon_t - \overline{\upsilon_\Delta}\right|}\sqrt{1 - \left[-\frac{2\left(\upsilon_t - \overline{\upsilon_\Delta}\right)^2}{\pi\sigma_\upsilon^2}\right]}\right), \tag{24}$$

so that

$$\upsilon_t = \overline{\upsilon_\Delta} + \sigma_\upsilon \frac{0.5 - p}{|0.5 - p|}\sqrt{\frac{\pi}{2}\ln\left[\frac{1}{4p(1-p)}\right]}, \tag{25}$$

where $0 < p < 1$. The mean $\overline{\upsilon_\Delta}$ and variance σ_υ^2 of υ_Δ can be estimated by first-order approximation using a Taylor series expansion, and then related to the mean and variance of u_Δ, giving

$$\overline{\upsilon_\Delta} = \ln\left[\overline{u_\Delta}\Big/\sqrt{1 + \left(\sigma/\overline{u_\Delta}\right)^2}\right] = \ln\left(u_*\,\overline{u_\Delta}^+\Big/\sqrt{1 + \left(\sigma^+/\overline{u_\Delta}^+\right)^2}\right), \tag{26}$$

$$\sigma_\upsilon^2 = \ln\left[1 + \left(\sigma/\overline{u_\Delta}\right)^2\right] = \ln\left[1 + \left(\sigma^+/\overline{u_\Delta}^+\right)^2\right]. \tag{27}$$

Combining eqs. (24), (26) and (27), we have

$$u_t = \frac{u_*\overline{u_\Delta}^+}{\sqrt{1 + \left(\sigma^+/\overline{u_\Delta}^+\right)^2}}\exp\left\{\frac{0.5 - p}{|0.5 - p|}\sqrt{\ln\left[1 + \left(\sigma^+/\overline{u_\Delta}^+\right)^2\right]}\sqrt{\frac{\pi}{2}\ln\left[\frac{1}{4p(1-p)}\right]}\right\}. \tag{28}$$

Therefore, substituting eq. (10) into eq. (28) and solving for the threshold friction velocity u_{*t} by setting $u_* = u_{*t}$, we have

$$u_{*t} = \frac{\sqrt{1+\left(\sigma^+ / \overline{u_\Delta}^+\right)^2}\sqrt{\dfrac{1}{C_D L_D + C_L L_L}\dfrac{\pi d^2}{3S\rho_f}\left((\rho_p-\rho_f)L_w g d + \dfrac{C_C L_C}{d}\right)}}{\overline{u_\Delta}^+ \exp\left\{\dfrac{0.5-p}{|0.5-p|}\sqrt{\ln\left[1+\left(\sigma^+ / \overline{u_\Delta}^+\right)^2\right]}\sqrt{\dfrac{\pi}{2}\ln\left[\dfrac{1}{4p(1-p)}\right]}\right\}}. \tag{29}$$

Substituting eq. (29) into $A = \rho_f u_{*t}^2 / (\rho_p - \rho_f) g d$, we have

$$A = f_p F_1 F_2 G(d), \tag{30}$$

where

$$f_p = \frac{L_w}{C_D L_D + C_L L_L}\frac{\pi d^2}{3S}, \tag{31}$$

$$F_1 = 1 \Big/ \left(\overline{u_\Delta}^+\right)^2, \tag{32}$$

$$F_2 = \left[1+\left(\sigma^+\right)^2 F_1\right] \Bigg/ \left(\exp\left\{\frac{0.5-p}{|0.5-p|}\sqrt{\ln\left[1+\left(\sigma^+\right)^2 F_1\right]}\sqrt{\frac{\pi}{2}\ln\left[\frac{1}{4p(1-p)}\right]}\right\}\right)^2, \tag{33}$$

and

$$G(d) = 1 + \frac{1}{(\rho_p-\rho_f)g}\frac{6C_C L_C}{\pi L_w}\frac{1}{d^2}, \tag{34}$$

All flow properties in eqs (28) to (34) are evaluated at the dimensionless reference height (y_Δ^+). In particular, from eqs. (13) and (14), $\overline{u_\Delta}^+$ is a function of y_Δ^+ and roughness Reynolds number k_s^+ , and from eq. (20), σ^+ is a function of y_Δ^+ and the flow Reynolds number Re_τ . However, at the threshold of grain motion, both y_Δ^+ and k_s^+ are directly proportional to the threshold particle Reynolds number Re_{*t} . Hence eq. (30) replaces eqs. (1) and (2) with the more general formulation

$$A = f_p F_1(\mathrm{Re}_{*t}) F_2(\mathrm{Re}_{*t}, \mathrm{Re}_\tau) G(d). \tag{35}$$

Eq. (35) states that the dimensionless threshold shear stress A is governed by four types of effect:

i) particle packing geometry, represented by the parameter f_p;

ii) the mean velocity profile (first-order flow effects), represented by $F_1(\mathrm{Re}_{*t})$;

iii) interaction between the mean velocity profile, turbulent fluctuations and particle removal probability p (second-order flow effects), represented by $F_2(\mathrm{Re}_{*t}, \mathrm{Re}_\tau)$; and

iv) inter-particle cohesion, represented by $G(d)$.

Ignoring the turbulent fluctuations (*i.e.* $\sigma^+ = 0$ and therefore $F_2 = 1$) and inter-particle cohesion (*i.e.* $C_C \to 0$ and therefore $G(d) \to 1$), we have $A \cong f_p F_1$. In this case, F_1 can be interpreted as a first-order effect of the flow that depends solely on the mean velocity profile $\overline{u_\Delta}^+$, which, in turn, depends only on Re_{*t}. For similar reasons, F_2 can be viewed as a second-order effect of the flow as it depends on the turbulent fluctuation σ^+. If we assume $A_1 = f_p$ (see eq. (2)), the main contribution of our new expression (35) is to introduce F_2, and further specify F_1 and $G(d)$. Note that the particle packing parameter f_p depends on the drag and lift coefficients C_D and C_L, which both depend on the choice of reference height y and Re_{*t}. Such dependences could be important in determining A and its variations. Certain aspects of the statistical effects of particle packing geometry have been discussed by *Wu and Chou* [2003] and *Papanicolaou et al.* [2002] and further research is needed to understand the effects of C_D and C_L in relation to Re_{*t}.

In this paper we focus on the effects of turbulent fluctuations on A. The statistical effect of the packing condition will not be considered, and f_p is treated as a constant, assuming a fixed packing geometry (Figure 2). Using parameter values defined in Section 2.1, we have $f_p \approx 1$ to 2. For simplicity, an average value of 1.5 is used throughout. In reality, F_1 and F_2 may also depend on particle packing conditions, but such effects are also excluded from this paper.

Several expressions have been proposed for the effect of inter-particle cohesion in the past. In general, they share a form similar to

$$G(d) = 1 + \frac{K_1}{(\rho_p - \rho_f) g d^{3-n}}, \tag{36}$$

where K_1 and n are parameters which need to be calibrated against data. With $n = 1$ and $K_1 = \frac{6 C_C L_C}{\pi L_w}$, eq. (36) reduces to eq. (34) and stands for the assumption of direct proportionality between the cohesion force F_C and particle size d. Values of the parameters n and K_1 from previous researchers are listed in Table 2. The resulting expressions for $G(d)$ are plotted in Figure 6. This shows that inter-particle cohesion becomes negligible when d > 100 μm (in air). However, cohesion is important in determining the upward trend in A with decreasing Re_{*t}, at $\mathrm{Re}_{*t} < 1$ (Figure 1).

From Table 2 and Figure 6, it can be inferred that it is reasonable (given earlier work) to assume F_C proportional to d, and that the most likely range of values for the cohesion coefficient C_C is between 10^{-6} and 10^{-4} N m^{-1}. Though the parameter values listed in Table 2 were all calibrated using

the wind tunnel data of *Iversen and White* [1982], they are consistent with values of C_C found in adhesion studies. For instance, C_C was found to be of the order of 10^{-4} ~10^{-2} N m^{-1} in air [*Corn*, 1961] and 10^{-6} ~10^{-4} N m^{-1} in water [*Zimon*, 1982]. Accordingly, the estimates provided in Table 2 may represent the lower bounds of such effects in air.

[[Insert Figure 6 here]]

Zimon [1982] attributed the different relationships between F_C and particle size d, resulting in a range of values of F_C for a given d, to the probabilistic nature of particle removal. The variance of F_C is larger for smaller particles, and may also be larger in air relative to water. For instance, for particle sizes in the range 10 to 20 μm in air, F_C at a particle removal probability of 50% can be 10^2 to 10^3 times larger than at a small removal probability (2% to 5%), while for particles smaller than 10 μm, the difference can be as large as 10^5 [see Fig. 1.2 of *Zimon*, 1982]. Therefore, for small particles, the effect of the cohesion force on the entrainment threshold is not clear, as a large uncertainty and high variance in A are expected in both experimental data and theoretical estimates for particle size smaller than 10 μm.

3 Results and Discussion

In this section we focus on the first- and second-order flow-related effects, F_1 and F_2, mainly considering the range $\mathrm{Re}_{*t} > 10$ where $G(d) \rightarrow 1$ (i.e. medium to larger particles). In Section 3.3, we compare our results with experimental data under a variety of different removal probabilities (p) and inter-particle cohesion parameter values (C_C). For all calculations, kinematic viscosity ν is set to 1.47×10^{-5} m^2 s^{-1} in air and 1.0×10^{-6} m^2 s^{-1} in water, particle density ρ_p to 2650 kg m^{-3}, and fluid density ρ_f to 1 kg m^{-3} in air and 1000 kg m^{-3} in water.

3.1. First-Order Effects - Effects of the Mean Velocity Profile

Figure 7 shows contour plots of F_1 in $k_s^+ \sim y_\Delta^+$ space (dashed lines), with equations accounting for all three flow regimes (eqs. (13), (14) and (15)) in Figure 7a, and for the fully-rough regime only (eqs. (16) and (19)) in Figure 7b. In general, these diagrams show that contour lines of F_1 are parallel to lines $k_s^+ = \zeta y_\Delta^+$, where ζ is a constant. F_1 reaches a maximum value of round 0.2 at ζ = 30. When ζ < 30, F_1 decreases with y^+ but increases with the roughness Reynolds number k_s^+, whereas when ζ > 30, F_1 increases with y^+ but decreases with k_s^+. In the region where ζ < 30, the opposite effects of k_s^+ and y_Δ^+ on F_1 (and therefore on the dimensionless shear stress A) are the main

reason that values of A are confined to a rather narrow range in both air and water. The region where $\zeta > 30$ may have little to do with threshold entrainment. These points should become increasingly clear later in this Section.

[[Insert Figure 7 here]]

The differences in F_1 between Figures 7a (using all three flow regimes) and Figure 7b (using only the fully-rough regime) are most evident when $k_s^+ \le 70$, where the flow is either smooth or transitionally rough. This is consistent with the findings of *Ligrani and Moffat* [1986] and *Raupach et al*. [1991]. In the smooth flow regime, values of F_1 are larger if the flow is treated as smooth rather than as fully rough. However, in the transitionally-rough regime, values of F_1 are smaller if the flow is treated as transitionally rough rather as fully rough. Therefore, A can be underestimated for small particles but overestimated for medium particles if fully-rough flow is assumed for all particle sizes. This implies that under/over-estimated values of A can arise as a result of the assumption of fully-rough flow, and explains why the experimental *Shields'* curve (Figure 1) dips in the vicinity of $\mathrm{Re}_{*_t} \sim 10$ to 30. This is most clearly seen in the data for water. *Iversen et al.* [1987] stated there is no indication of such a "dip" in A with Re_{*_t} for their own and others' data in air. This may be because fully rough flow is assumed for all atmospheric boundary layer studies [*Jiménez*, 2004], including the wind tunnel studies of *Iversen* and his colleagues.

In terms of threshold entrainment, the ratio between the equivalent sand roughness k_s and the particle diameter d, namely $\alpha = k_s/d$, has been discussed by *Ling* [1995], who indicated that α may be interpreted as a measure of the packing density of roughness elements. For threshold conditions, $\alpha = 0.3$ to 4 [*Ling,* 1995, *Cheng and Chiew*, 1998], implying that $k_s^+ = \alpha \mathrm{Re}_{*_t}$. Commonly used values of α are 1 for uniformly-sized particles and 2 for mixed particle sizes [*Wu and Lin*, 2002; *Wu and Chou*, 2003]. On the other hand, according to Section 2.1, $y = \beta d$, implying $y_\Delta^+ = \beta \mathrm{Re}_{*_t}$, where β lies between 0.5 and 1. We then have $k_s^+ = \zeta y_\Delta^+$, where $\zeta = \alpha/\beta$ varies approximately between 0.15 and 4. Larger values of ζ are possible for other types of packing geometry, as the packing geometry shown in Figure 2 represents the most exposed position for a sphere resting on a surface. Nevertheless, the contour lines outside of $\zeta = 0.1$ and $\zeta = 10$ may have little relevance for threshold entrainment.

Some typical cases of threshold entrainment are shown in Figure 7. They are $\zeta = 0.5$, 1, 2 and 4, respectively (solid lines). The upper bound of particle size common in gravelly fluvial systems is a grain size of about 100 mm [*Graf*, 1971; *Buffington and Montgomery*, 1997], whereas it is two

orders of magnitude smaller in aeolian systems [*Bagnold*, 1941; *Greeley and Iversen*, 1985]. Thus, the approximate upper bounds of k_s^+ and y_Δ^+ are of the order of 10^4 for fluvial systems (the lightly-shaded area), and approximately 10^2 for aeolian systems (dark shading), respectively. This shows that, in air, threshold particle motion is likely to occur within the transitionally-rough and smooth regimes, rather than in the fully-rough regime. It also shows that, for $\zeta = 0.5 \sim 4$, the values of F_1 are mainly limited to $0.01 \sim 0.05$. Multiplying these values by $f_p = 1.5$ gives values of A as expected for fluvial entrainment [*Graf*, 1971; *Qian and Wan*, 1983; *Buffington and Montgomery*, 1997], but slightly larger than those obtained in wind tunnels [*Bagnold*, 1941; *Iversen and White*, 1982]. The physical cause of such differences will be investigated further in Section 3.2.

In comparison to uniformly-sized beds, α tends to become larger and β tends to become smaller for mixed particle beds due to the hiding effect. As has been assumed previously by other researchers, for a given average bed particle size, $\zeta = 0.5 \sim 1$ represents more uniformly-sized beds, and a larger ζ represents mixed-sized surfaces [*Wu and Lin*, 2002; *Wu and Chou*, 2003]. Figure 7 provides a theoretical explanation for the observation that A for mixed particle sizes is often larger than that for uniformly sized particles [*Shields*, 1936; *Buffington and Montgomery*, 1997]. In addition, as particle sorting processes cause both α and β to vary spatially and temporally, they inevitably increase the variations of A [*Church*, 1978; *Andrews*, 1983]. This explains why the "dip" in A disappears in data obtained from mixed-sized river beds.

3.2. Second-Order Effects - Effects of Boundary Layer Friction Reynolds Number Re_τ

The mean streamwise velocity is not the only factor affecting threshold entrainment. The turbulent velocity is also responsible for the initial dislodgement of sediment. Eq. (33) provides us the means to investigate the second-order effects on A due to turbulent fluctuations, through the effects of bulk Reynolds number and its relation to particle removal probability. In order to understand the general effect of turbulent fluctuations on A, and for simplicity, $\sigma^+ = \sigma^+_{\max}$ is assumed at the height of the mean threshold velocity $\overline{u_\Delta}$ and is applied to all particle sizes. Eq. (21) is used to relate the maximum turbulent fluctuation $\sigma^+_{\max}$ to Re_τ.

[[Insert Figure 8 here]]

Figure 8 shows contour plots of F_2 in $\sigma^+ \sim p$ space with F_1 set to 0.01, 0.03 and 0.06 (left to right panels, respectively). For all three cases, F_2 increases with removal probability p. This shows that, for any given Re_τ, F_2 has values smaller than 1 for $0 < p < 0.3$ and larger than 1 for $0.3 < p < 1$. Thus, F_2 acts to increase the variation of A. If we assume that $A = f_p F_1$ (as analyzed in Section 3.1)

represents the mean, multiplying this quantity by F_2 reduces the actual value of A when $0 < p < 0.3$ but enlarges it when $0.3 < p < 1$.

Figure 8 also shows that F_2 increases gradually with Re_τ when $0 < p < 0.3$, and that this increase is more noticeable for smaller values of F_1 than for larger ones. Physically, we would expect this to happen as the larger the turbulent fluctuations, the easier the initial dislodgement of sediment, and therefore, the greater the amount of reduction in A in comparison to its mean. We argue that this represents another reason for smaller values of A in air than those obtained in water (Figure 1). According to Figure 5, at the threshold, we may assume that $\mathrm{Re}_{\tau,w} = 500$ in flumes and $\mathrm{Re}_{\tau,a} = 50000$ in wind tunnels respectively. Figure 9 shows the estimated values of $F_{2,w}$, $F_{2,a}$ and their ratio $\eta = F_{2,\mathrm{w}}/F_{2,a}$ in relation to p, with $F_{1,w} = F_{1,a} = 0.01$ and 0.04, respectively. The slope of the $F_2 \sim p$ relationship is larger in air than that is in water. The two $F_2 \sim p$ relationships intersect at approximately $p = 0.2 \sim 0.3$, and F_2 in air is about half of its value in water for $p = 0.01 \sim 0.05$. The phenomenon that particle entrainment in air is easier for a smaller removal probability, but progressively harder for a larger removal probability for the same particle size entrained by water has also been found experimentally by *Zimon* [1982]. However, the explanation provided by *Zimon* [1982] was based upon the probabilistic nature of particle cohesion rather than statistical properties of near-wall turbulence, as argued here.

[[Insert Figure 9 here]]

Figure 1 suggests that the difference in A between air and water is actually larger than that predicted in Figure 9. This can be attributed to the following reasons. Firstly, it is because of different definitions of particle removal probability at the threshold. Particle removal probabilities at the threshold are never clearly defined under experimental conditions. For instance, those values of A lower than 0.04 were obtained by visual observations, in comparison to those obtained using bedload transport rates [*Buffington and Montgomery*, 1997]. Secondly, it is shown in Section 3.1 that the average F_1 may be larger in water than in air. In fact, data reported in Figure 1 are mostly averaged from different experiments with similar conditions. If we assume $F_{1,w} = 2F_{1,a}$, $f_{p,w} = f_{p,w}$ and $G_a(d) = G_w(d) = 1$ (applicable for medium to large particles), then A_w would be approximately 3 to 4 times larger than A_a at $p = 0.02$. Such a ratio is close to what is seen in Figure 1.

Previous analyses in hydraulic literature treat the instantaneous pick-up velocity u_t and its fluctuation σ as linearly proportionality to the friction velocity u_*, *i.e.* $u_t = C_t u_*$ and $\sigma = C_\sigma u_*$, where C_t and C_σ are constants with values of approximately 5.5 and 2.0, respectively [*Kironoto and Graf*, 1994; *Cheng and Chiew*, 1998; *Wu and Lin*, 2002]. Also, fully-rough turbulent flow is

assumed with no allowance for variations in σ. A constant value of σ fails to predict the systematically lower values of A at large Re_{*t} observed in air, in comparison to those observed in open channel flow. In this study, σ is allowed to vary with bulk Reynolds number as expressed by eqs. (20) and (21). Therefore, linking incipient motion to the scaling of turbulent fluctuation σ is the key contribution of this study as this provides us with a fundamental basis to explain the systematically lower values of A in air than in water.

The smaller values of A for smaller removal probabilities in air (and larger values for larger probabilities) suggest that the variance of threshold velocity is larger in air than it is in water. This may have profound implications for understanding wind erosion and aeolian transport. For instance, wind tunnel studies of *Shao et al*. [1993] found that dust emission is mainly due to saltation bombardment, and that dust emission arising from direct aerodynamic entrainment is generally small. On the other hand, direct field observations of *Loosmore and Hunt* [2000] found dust suspension can be initialized by turbulent eddies in surface winds well before the sandblasting mechanism. Similar observations were made by *Roney and White* [2004] at Owens Lake. Both *Loosmore and Hunt* [2000] and *Roney and White* [2004] found that the threshold velocity is smaller than the values estimated by the conventional "saltation thresholds". From Figure 8 and 9, we suggest that the physical causes of the discrepancy are likely to be due to the different definitions of the threshold removal probability. While *Shao et al*. [1993] looked at sustained dust emission rates at an average p (at approximately 30% to 50%), the latter two studies focused on initial uplifting at $p = 1 \sim 10\%$.

Figures 7 and 8 also show that F_1 may also affect F_2. At smaller p, the effect of Re_τ on A becomes less evident when F_1 becomes larger. Also, for a given p, F_2 increases with F_1. Physically, this means that when A is larger, there is less reduction in its value by the second-order effect (*i.e.* when multiplying it by F_2). Further experimental studies are needed to investigate these findings. In reality, the effects of Re_τ and Re_{*t} are more complex than those presented in Figures 7 and 8. This is because A, Re_τ and Re_{*t} are all related to threshold velocity u_{*t}, which increases with particle size. In addition, boundary layer height δ may change with particle size.

Direct field measurements by *Roney and White* [2004] at Owens Lake found that the dust suspension threshold varied between 50 and 75% of the values estimated from expressions derived from wind tunnel experiments. The general model proposed in this study provides the physical explanation for such an observation. Figure 10 shows three possible $A \sim \mathrm{Re}_{*t}$ relationships at boundary layer heights of $\delta = 0.01$ m, 1 m, and 1000 m, respectively, all for $p = 0.05$. These curves were obtained, for an in-air situation, by substituting eqs. (13) and (20) in eqs. (32) and (33) with

$y_\Delta^+ = 0.6\mathrm{Re}_{*t}$, $k_s^+ = \mathrm{Re}_{*t}$ and $C_C = 4 \times 10^{-5}$ N m^{-1}. The values of A were calculated through iteration over u_{*t} for a given particle size d. This shows that A decreases with δ and the decrement increases when Re_{*t} increases, suggesting that, for the same values of Re_{*t}, direct field measurement would result in smaller A in comparison to that in wind tunnel conditions. The physical implication is that, for a given particle size, the average threshold velocity for dislodging particles could be smaller in the atmospheric boundary layer compared with that observed in wind tunnels. Alternatively, a particle that remains still in a wind tunnel may move if it is in an atmospheric boundary layer at the same wind velocity.

[[Insert Figure 10 here]]

3.3. Comparison with Experimental Data

In this section, using an approach similar to that employed to derive Figure 10, we shall use eqs. (13) and (20) to estimate F_1 and F_2. A is then calculated through iteration over u_{*t} for a given particle size d. For all calculations below, we assume $y_\Delta^+ = 0.6\mathrm{Re}_{*t}$. When comparing predictions with data from flume experiments, we assume $k_s^+ = 3\mathrm{Re}_{*t}$ and $\delta = 0.02$ m, while $k_s^+ = \mathrm{Re}_{*t}$ and $\delta = 1.2$ m for comparing with data from wind tunnels.

Figure 11 shows predicted $A \sim \mathrm{Re}_{*t}$ relationships for four values of p in air and in water and three values of the cohesion coefficient C_C, respectively. For a given fluid, the variation of A in relation to Re_{*t} can be explained by differences in the removal probability p when $\mathrm{Re}_{*t} > 10$, by inter-particle cohesion when $\mathrm{Re}_{*t} < 1$, and by both of them when Re_{*t} is in between. The Figure shows that, with a mean value of $C_C = 10^{-5} \sim 10^{-4}$ N m^{-1}, the new expression agrees very well with experimental data for both air and water. The C_C values used in this study are smaller than those suggested previously [*Shao and Lu*, 2000; *Cornelis and Gabriels*, 2004], but this is because flow-related effects play an increasingly important role in the new expression we propose. As discussed in Section 3.1 and shown in Figure 7, at smaller k_s^+ and y_Δ^+ (therefore smaller Re_{*t}), F_1 (therefore A) increases with Re_{*t}.

[[Insert Figure 11 here]]

Previous researchers have suggested that the particle-to-fluid density ratio $R_\rho = \left(\rho_p - \rho_f\right)/\rho_f$ is an important parameter in determining A [*Iversen et al.*, 1987; *Cornelis and Gabriels*, 2004]. Our new expression suggests that A also depends on both Re_{*t} and Re_τ, not just on R_ρ. Therefore, in terms of the effects of flow on A, not only the density but also the flow viscosity is important. For a set of

fixed values of viscosity, particle size, and boundary layer height, our new expression suggests that A increases when R_ρ decreases, as was shown by the wind tunnel data of *Iversen and White* [1982]. However, it would no longer be these parameters also vary, according to our generalized model. The experimental simulations of *McKenna Neuman* [2003; 2004] confirm that A and sediment transport rates depend not only on fluid density (or R_ρ) but also on fluid viscosity. She showed both threshold velocity and mass transport rates of sedimentary particles vary with temperature (Selby *et al*., 1974) and humidity. For instance, it was found that the aerodynamic drag required to entrain sand size particles can be 30% lower under cold conditions in high latitude regions, as compared to hot deserts and mass transport rates increase while temperature decreases. *McKenna Neuman* [2004] suggested that temperature-dependent changes in air density and viscosity, and turbulence, are the major affecting factors. This example shows that caution is needed in applying previous analytical and semi-empirical models, and in assuming fixed parameter values, as both models and parameters may only be applicable to certain conditions.

Both theoretical analysis and observation show a certain degree of variation in A. We therefore argue that threshold entrainment should be viewed statistically rather than deterministically, as most governing processes are probabilistic in nature, including near-surface turbulent flow, packing geometry [*Kirchner et al.*, 1990; *Papanicolaou et al*., 2002] and inter-particle cohesion. For instance, the most important process – rough wall turbulent motion – is fundamentally stochastic. The structure of near-bed turbulent flow is characterized by the spatial and temporal organization of coherent structures [*Best*, 1992], the links between outer and inner scales, the nature of intermittency and the role of anisotropy. All these turbulence characteristics depend on and interact with the bed condition in a complex manner. In addition, for small values of Re_{*t}, the interparticle cohesion forces are also statistical in nature, and the relationships between cohesion forces and particle size are very complex and not well understood (see Section 2.1). For all these reasons, a deterministic resolution of incipient motion may not be possible. This message is particularly relevant to wind erosion studies where a deterministic view of incipient motion remains common, and data on incipient motion are too sparse to separate the variety of physical processes involved.

4 Conclusions

In this study, we have proposed a new, general expression for the dimensionless threshold shear stress A which is applicable to both aeolian and fluvial particle entrainment. It allows us to study the effects of mean flow, turbulent fluctuation, and inter-particle cohesion on incipient motion separately. It suggests that the dimensionless threshold shear stress A is indeed related to Re_{*t}, as

earlier researchers proposed, and should also depend on flow Reynolds number Re_τ, which is proposed for the first time. Therefore, A depends on the flow *condition* and it should be a function of the viscosity (a flow *property*) as well as being a function of the density ratio and particle size.

We have shown that the differences in the probability distribution of streamwise velocity fluctuations for typical situations in air and water are the main reason for the larger values of A in water than in air (Figure 1). This is because the turbulent fluctuations are not only related to the near-bed flow structure (*i.e.* Re_{*t}), as expected, but also depend on the bulk flow characteristics (*i.e.* Re_τ). As velocity variance increases with the bulk flow Reynolds number Re_τ, and typical values of Re_τ in air are several orders larger than those in water under the conditions of incipient motion, so the values of A are smaller in air than in water. The upturn of A for small Re_{*t} is partly due to the flow conditions and partly due to inter-particle cohesion. Therefore, incorporating descriptions of the flow condition into threshold entrainment is indispensable for *all* particle sizes.

At large Re_{*t}, the narrow range of values of A in relation to Re_{*t} results from the opposite effects of the roughness Reynolds number k_s^+ and the dimensionless reference height y_Δ^+, both of which are proportional to the particle Reynolds number Re_{*t}. Although the mean values of A may be within a narrow range, certain systematic variations exist. These variations are due to differences in particle packing density, which is incorporated in the first-order effect F_1; and to the different removal probability (p) used in different experiments, and the bulk Reynolds number, which are incorporated in the second-order effect F_2. In reality, these effects are likely to act interactively on A and are reflected in a combined but rather random manner in experimental studies.

ACKNOWLEDGEMENTS

HL is grateful to Professor Herbert Huppert at The Institute of Theoretical Physics, University of Cambridge, for his kind support. We would like to thank two anonymous reviewers for their thoughtful comments, which greatly improved this paper.

References

Andrews, E. D., Entrainment of gravel from naturally sorted riverbed material, *Geol. Soc. Am. Bull*., 94, 1225–1231, 1983.

Bagnold, R. A., *The physics of blown sand and desert dunes*, Methuen, London, 1941.

Bagnold, R. A., The flow of cohesionless grains in fluids, *Philosophical Trans. Roy. Soc. London*, *A*, 249 No.964, 1956.

Barenblatt, G. I., and A. J. Chorin, Scaling of the intermediate region in wall-bounded turbulence: The power law. *Phys. Fluids*, 10, 1043–1044, 1998.

Batchelor, G. K., *An introduction to fluid dynamics*, Cambridge University Press, Cambridge, 615pp, 1967.

Best, J. L., On the entrainment of sediment and initiation of bed defects: insights from recent developments within turbulent boundary layer research. *Sedimentology*, 39, 797–811, 1992.

Bridge, J. S., and S. J. Bennett, A model for the entrainment and transport of sediment grains of mixed sizes, shapes, and densities, *Water Resours. Res.*, 28(2), 337–363, 1992.

Buffington, J. M., and D. R. Montgomery, A systematic analysis of eight decades of incipient motion studies, with special reference to gravel-beded rivers, *Water Resour. Res.*, 33, 1993–2029, 1997.

Bergstrom, D. J., M. F. Tachie, and R. Balachandar, Application of power laws to low Reynolds number boundary layers on smooth and rough surfaces, *Phys. Fluids*, 13(11), 3277–3284, 2001.

Cheng, N. S., and Y. M. Chiew, Pickup probability for sediment entrainment, *J. Hydraul. Eng.*, 124(2), 232–235, 1998.

Chepil, W. S., The use of evenly spaced hemisphere to evaluate aerodynamic forces on a soil surface, *Trans. Am. Geophys. Union*, 39(3), 397–404, 1958.

Church, M., Palaeohydrological reconstructions from a Holocene valley fill, In: Miall, A. D. (Ed.), Fluvial Sedimentology, *Can. Soc. of Pet. Geol*., Calgary, Alberta. 743–772, 1978

Clauser, F. H., The turbulent boundary layer, *Adv. Appl. Mechs.,* 4, 1-51, 1956.

Cleaver, J. W., and B. Yates, Mechanism of detachment of colloidal particles from a flat substrate in a turbulent flow, *J. Colloid Interface Sci.*, 44:464–474, 1973.

Coleman, N. L., A theoretical and experimental study of drag and lift forces acting on a sphere resting on hypothetical stream bed, *Proc., 12th compress,* IAHR, Fort Collins, Colo., 3, 185–192, 1967.

Corn, M., Adhesion of solid particles to solid surface, I: A review, *J. Air Pollution Control Assoc.*, 11, 523–537, 1961.

Cornelis, W. M., and D. Gabriels, A simple model for the prediction of the deflation threshold shear velocity of dry loose particles, *Sedimentology*, 51, 39–51, 2004.

Einstein, H. A., *The bed load function for sediment transportation in open channel flows*, Tech. Bull. 1026, USDA, Washington, D.C, 1950.

Fischer, P., G. Leaf, and J. Restrepo, Forces on particles in oscillatory boundary layers, *J. Fluid Mech.*, 468, 327–347, 2002.

Fletcher, B., The erosion of dust by an airflow, *J. Phys. D: Appl. Phys*., 9, 913–524, 1976a.

Fletcher, B., The incipient motion of granular materials, *J. Phys. D: Appl. Phys*., 9, 2471–2478, 1976b.

Fuks, N. A., *Aerosol Mechanics*, 358pp, Nauka, Moscow, 1955.

DeGraaff, D. B., and J. K. Eaton, Reynolds number scaling of the flat plate turbulent boundary layer, *J. Fluid Mech*., 422, 319–346, 2000.

Gessler, J., Beginning and ceasing of sediment motion, In: H. W. Shen (Ed.), *River mechanics*, Fort Collins, Colo., 7:1–7:22, 1971.

Graf, W. H., *Hydraulics of Sediment Transport*, McGraw-Hill Book Company, New York, 1971.

Grass, A. J., Initial instability of fine sand, *J. Hydraul. Div.*, *Am. Soc. Civ. Eng*., 96(3), 619–632, 1970.

Greeley, R., and J. D. Iversen, *Wind as a Geological Process on Earth, Mars, Venus and Titan*, Cambridge University Press, New York, 1985.

Iversen, J. D. and B. R. White, Saltation threshold on Earth, Mars and Venus, *Sedimentology*, 29, 111–119, 1982.

Iversen, J. D., R. Greeley, J. R. Marshall, and J. B. Pollack, Aeolian saltation threshold: the effect of density ratio, *Sedimentology*, 34, 699–706, 1987.

Jackson, P. S., On the displacement height in the logarithmic velocity profile, *J. Fluid Mech*., 111, 15–25, 1981.

James, C., Prediction of entrainment conditions for nonuniform, noncohesive sediments, *J. Hydraul. Res.* 28(1), 25–41, 1990.

Jiménez, J., Turbulent Flows over Rough Walls, *Ann. Rev. Fluid Mech.*, 36, 173–96, 2004.

Kirchner, J. W., W. E. Dietrich, F. Iseya, and H. Ikeda, The variability of critical shear stress, friction angle, and grain protrusion in water-worked sediments, *Sedimentology*, 37, 647-672, 1990.

Kironoto, B. A., and W. H. Graf, Turbulence characteristics in rough uniform open-channel flow, *Proc. Inst. Civ. Eng., Water, Maritime Energ.*, 106, 333–344, 1994.

Komar, P.D. and Li, Z., Applications of grain-pivoting and sliding analyses to selective entrainment of gravel and flow competence evaluations. *Sedimentolog*y, 35, 681-695.

Krogstad, P. A., and R. A. Antonia, Surface roughness effects in turbulent boundary layers, *Exp. Fluids*, 27, 450–460, 1999.

Ligrani, P. M., and R. J. Moffat, Structure of transitionally rough and fully rough turbulent boundary layers, *J. Fluid Mech.*, 162, 69–98, 1986.

Ling, C. H., Criteria for incipient motion of spherical sediment particles, *J. Hydraul. Eng.,* 121(6), 47–478, 1995.

Loosmore, G. A., and J. R. Hunt, Below-threshold, non-abraded dust resuspension, *J. Geophy. Res.*, 105, 20663–20671, 2000.

Mantz, P., Incipient transport of fine grains and flakes by fluids – Extended Shields diagram, *J. Hydraul. Div. Am. Soc. Civ. Eng*., 103(6), 601–615, 1977.

Marsh, N. A., A.W. Western, and R. B. Grayson, Comparison of methods for predicting incipient motion for sand beds, *J. Hydraul. Eng.*, 130(7), 616–621, 2004.

Marusic, I., and G. J. Kunkel, Streamwise turbulence intensity formulation for flat-plate boundary layers, *Phys. Fluids*, 15(8), 2461–2464, 2003.

McKenna Neuman, C., Effects of temperature and humidity upon the entrainment of sedimentary particles by wind, *Boundary-Layer Meteorology*, 108, 61–89, 2003.

McKenna Neuman, C., Effects of temperature and humidity upon the transport of sedimentary particles by wind, *Sedimentology*, 51, 1–18, 2004.

Metzger, M., J. Klewicki, K. Bradshaw, and R. Sadr, Scaling the near-wall axial turbulent stress in the zero pressure gradient boundary layer, *Physics of Fluids*, 13, 1819–1821, 2001.

Morrison, J. F., B. J. McKeon, W. Jiang, and A. J. Smits, Scaling of the streamwise velocity component in turbulent pipe flow, *J. Fluid Mech*., 508, 99–131, 2004.

Nickling, W. G., The initiation of particle movement by wind, *Sedimentology*, 35, 499–511, 1988.

Nikuradse, J., Strömungsgesetze in Rauhen Rohren, *VDI-Forsch*. 361, 1933 (Engl. transl. 1950. Laws of flow in rough pipes, NACA TM 1292).

Panton, R., Review of wall turbulence as described by composite expansions, *Applied Mechanics Reviews, Trans. ASME*, 58, 1–36, 2005.

Papanicolaou, A., P. Diplas, C. L. Dancey, and M. Balakrishnan, Surface roughness effects in near-bed turbulence: Implications to sediment entrainment, *J. Eng. Mech*., 127(3), 211–218, 2001.

Papanicolaou, A. N., P. Diplas, N. Evaggelopoulos, and S. Fotopoulos, Stochastic incipient motion criterion for spheres under various bed packing conditions, *J. Hydraul. Eng.*, 128(4), 369–380, 2002.

Patnaik, P. C., N. Vittal, and P. K. Pande, Lift coefficient of a stationary sphere in gradient flow, *J. Hydraul. Res.,* 32(3), 471–480, 1994.

Phillips, M., A force balance model for particle entrainment into a fluid stream, *J. Phys. D: Appl. Phys.*, 13, 221–233, 1980.

Qian, N., and C. H. Wan, *Mechanics of sediment transport*, Science press, Beijing (in Chinese), 1983 (Engl. Transl. by J. S. McNown, 1998, American Society of Civil Engineers).

Raupach, M. R., Drag and drag partition on rough surfaces, *Boundary-Layer Meteorol*., 60, 375-395, 1992.

Raupach, M. R., R. A. Antonia, and S. Rajagopalan, Rough-Wall Turbulent Boundary Layers, *Appl. Mech. Rev.,* 44, 1–25, 1991.

Raupach, M. R., and H. Lu, Representation of land-surface processes in Aeolian transport models, *Environ. Modelling & Software*, 19, 93–112, 2004.

Raupach, M.R., J.J. Finnigan and Y. Brunet, Coherent eddies and turbulence in vegetation canopies: the mixing layer analogy, *Boundary-Layer Meteorol*. 78, 351-382, 1996.

Richards, K.S., Fluvial geomorphology: initial entrainment of bed material in gravel-bed rivers. *Progress in Physical Geography*, 14, 395-415, 1990.

Roney, J. A., and B. R. White, Definition and measurement of dust aeolain thresholds, *J. Geophys. Res.*, 109, F01013, doi: 10.1029/2003KF000061, 2004.

Selby, M. J., R. B. Rains, and R. W. P. Palmer, Eolian deposits of the ice-free Victoria Valley, Southern Victoria Land and Antarctica. *New Zealand Journal of Geology and Geophysics*, 17(3), 543-562, 1974

Shao, Y., and H. Lu, A simple expression for wind erosion threshold friction velocity, *J. Geophy. Res.*, 105, 22437–22443, 2000.

Shao, Y., M. R. Raupach, and P. A. Findlater, The effect of saltation bombardment on the entrainment of dust by wind, *J. Geophy. Res*., 98, 12719–13726, 1993.

Shields, A., Application of similarity principles and turbulence research to bed-load movement (in German), *Preuss. Vers. Anst. Wasserb. Schiffb*., No. 26, Berlin, 1936.

Tachie, M. F., D. J. Bergstrom, and R. Balachandar, Roughness effects on the mixing properties in open channel turbulent boundary layers, *J. Fluids Eng*., 126, 1025–1032, 2004.

Theodoor, J., and G. Overbeek, Birth, life and death of colloids, In: Eicke, E. H.-F. (Ed.), *Modern Trends in Colloid Science in Chemistry and Biology*, 9–33. Springer-Verlag, 1985.

Tillman, W., Neue Widerstandsmessungen an Oberflächenstörunden in der turbulenten Reibungsschicht, *ZWB Untersuch. Mitteil*. 6619, 1944 (Engl. Transl. 1951, Additional measurements of the drag of surface irregularities in turbulent boundary layers. NACA TM 1299).

Wu, F. C., and Y. J. Chou, Rolling and lifting probabilities of sediment entrainment, *J. Hydraul. Eng.*, 129(2), 110–119, 2003.

Wu, F. C., and Y. C. Lin, Pickup probability of sediment under Log-normal velocity distribution, *J. Hydraul. Eng.*, 128(4), 438–442, 2002.

White, S. J., Plane bed thresholds of fine grained sediments, *Nature*, 228, 152–153, 1970.

Yalin, M. S., *Mechanics of sediment transport*, Pergamon Press, Oxford, 1972.

Yalin, M. S., and E. Karahan, Inception of sediment transport, *J. Hydraul. Div.*, *Am. Soc. Civ. Eng.*, 105, 1433–1443, 1979.

Zimon, D. Z., *Adhesion of Dust and Powder*, Translated by R. K. Johnston, Consultants Bureau, Plenum Press, New York, 1982.

Zingg, A.W., Wind tunnel studies of the movement of sedimentary material, *Proceedings 5th Hydraulic Conference Bulletin*, 34, 111–35, 1953.

Table 1. Main symbols (omitting symbols used only once)

Symbol	Definition	First use
A	dimensionless threshold shear stress, $A = \rho_f u_{*t}^2 \big/ \left((\rho_p - \rho_f) g d\right)$	Eq (1)
A_1	reference value of A	Eq (2)
B	empirical constant in logarithmic law over a smooth wall ($B = 5.0$)	Eq (12)
c_i	cohesion coefficient	Eq (6)
C_D, C_L	drag, lift coefficients (computations assume $C_D = 0.5$, $C_L = 0.3$)	Eqs (4), (5)
d	particle diameter	Eq (1)
F_D, F_L, F_G, F_C	forces on particle from drag, lift, specific weight and cohesion	Eqs (3) to (5)
$F(\mathrm{Re}_{*t})$	dimensionless function quantifying dependence of A on gravitational and aerodynamic forces	Eq (2)
f_p	component of F associated with packing geometry (computations assume $f_p = 1.5$)	Eq (31)
F_1	component of F associated with first-order flow effects	Eq (32)
F_2	component of F associated with second-order flow effects	Eq (33)
$G(d)$	dimensionless function quantifying dependence of A on cohesion forces	Eq (2)
g	gravitational acceleration	Eq (1)
k_s	Nikuradse sand-grain roughness	Eq (14)
K_1	dimensional parameter for cohesion force	Eq (36)
L_D, L_L, L_G, L_C	moment arms for forces F_D, F_L, F_G, F_C ($L_D = d\cos\theta$, $L_L = d\sin\theta$, $L_G = d\sin\theta$ and $L_C = d\sin\theta$)	Eq (8)
n	exponent specifying cohesion force	Eq (36)
p	probability of entrainment	Eq (23)
Re_τ	flow Reynolds number, $\mathrm{Re}_\tau = u_* \delta / \nu$	Sec 2.3
Re_{*t}	particle Reynolds number at threshold, $\mathrm{Re}_{*t} = u_{*t} d / \nu$	Eq (1)
S	horizontal area of particle exposed to the flow (computations assume $S = 0.2\pi d^2$)	Eqs (4), (5)
u	streamwise velocity (dimensionless form: $u^+ = u/u_*$)	Sec 2
u_Δ	reference velocity (at height y_Δ) for defining F_D and F_L	Eqs (4), (5)
u_t	threshold velocity (at height y_Δ)	Eq (10)
u_{*t}	threshold friction velocity	Eq (1)
υ_Δ, υ_t	$\upsilon_\Delta = \ln u_\Delta$, $\upsilon_t = \ln u_t$	Eq (22)
y	height above level of effective drag ($y = 0$)	Sec 2
y^+	dimensionless height, $y^+ = u_* y / \nu$	Sec 2
y_Δ	height at which velocity u_Δ is defined	Eqs (4), (5)
y_Δ^+	dimensionless reference height at which velocity u_Δ is defined	Sec 2
z_0	roughness length	Eq (16)
z_i	smallest separation between two spherical particles in Eq. (6)	Eq (6)
β	constant relating reference height y_Δ to d	Sec 2.1
δ	boundary-layer depth	Sec 2.3
$\Delta\overline{u}^+$	velocity-increment form of roughness function	Eq (13)

κ	von Karman constant (κ = 0.41)	Eq (12)
ν	kinematic viscosity of the fluid.	Eq (1)
ξ	Interpolation function for roughness in transition regime	Eq (15)
ρ_f, ρ_p	fluid density, particle density	Eq (1)
θ	pivoting angle (see Figure 2; computations assume $\theta = 30^o$)	Eq (8)
σ	standard deviation of streamwise velocity (dimensionless form: $\sigma^+ = \sigma/u_*$)	Eq (20)
τ_{*t}	threshold shear stress, $\tau_{*_t} = \rho_f u_{*_t}^2$	Eq (1)

Table 2. Parameter values for eq. (36) and implied values of the cohesion parameter C_C.

K_1	C_C	n	Researchers
6×10^{-7} N m$^{-0.5}$	3.1×10^{-7} N m$^{-0.5}$	1.5	*Greeley and Iversen* [1985]
0.055*	0.029	1	*Iversen et al*. [1987]
1.65×10^{-4} to 5.0×10^{-4} N m^{-1}	8.6×10^{-5} to 2.6×10^{-4} N m^{-1}	1	*Shao and Lu* [2000]
1.69×10^{-4} to 1.77×10^{-4} N m^{-1}	8.8×10^{-5} to 9.3×10^{-5} N m^{-1}	1	*Cornelis and Gabriels* [2004]
7×10^{-6} N m$^{-1.3}$	3.7×10^{-6} N m$^{-1.3}$	1.3	*Cornelis and Gabriels* [2004]

* Note that the unit of K_1 was not specified in *Iversen et al*. [1987].

Figure Captions

Figure 1. Dimensionless threshold shear stress A as a function of particle Reynolds number Re_{*t}. The diagram shows that data obtained in water flow follow a different trend compared with those obtained in air stream. Data were extracted from the literature indicated in the legend.

Figure 2. Schematic of an erodible particle resting on other similar particles. Forces acting on the shaded particle include the aero/hydro-dynamic drag, F_D, the aero/hydro-dynamic lift $F_{L,}$ the gravitational force, F_G, and the net cohesive force, F_C. The vertical distribution of stream-wise mean velocity $\overline{u}$ is also shown.

Figure 3. Schematic diagram of probability of entrainment p equal to probability of exceedance $\mathrm{Prob}(u_\Delta \geq u_t)$, where u_Δ and u_t are the instantaneous reference velocity and the threshold velocity, respectively.

Figure 4. Normalized stream-wise turbulence intensities σ^+ as a function of normalized vertical height y^+ and boundary layer friction Reynolds number Re_τ. The lines are calculated using eq. (20).

Figure 5. Peak values of σ^+ from Figure 4 as a function of Re_τ. Typical ranges of Re_τ for flumes, natural rivers, wind tunnels and atmospheric boundary layers are also shown.

Figure 6. Previously published relationships of $G(d)$ as a function of particle size d.

Figure 7. Contour plots of F_1 in $y^+ \sim k_s^+$ space. In (a) eqs. (13) to (15) were used for the calculation; in (b) eq. (16) with $z_0/k_s = 0.031$ was used for the calculation. Note that y^+ is replaced by y_Δ^+ for the threshold condition of grain motion. See text for details.

Figure 8. Contour plot of F_2 in $\mathrm{Re}_\tau \sim p$ space. From left to right, the panels are for $F_1 = 0.01$, 0.03, and 0.06, respectively.

Figure 9. Left panels: F_2 as a function of p for the cases of air and water for $F_1 = 0.01$ (upper panel) and $F_1 = 0.04$ (lower panel). Right panels: the ratio of F_2 in water and air for the same F_1 values as on the left.

Figure 10. Computed $A \sim \mathrm{Re}_{*t}$ relationship in air for three different values of boundary layer height δ.

Figure 11. Comparison between computed $A \sim \mathrm{Re}_{*t}$ relationships in air and water. Dots shown are experimental data as in Figure 1, complemented by other data obtained from flume experiments [*Buffington and Montgomery*, 1997].

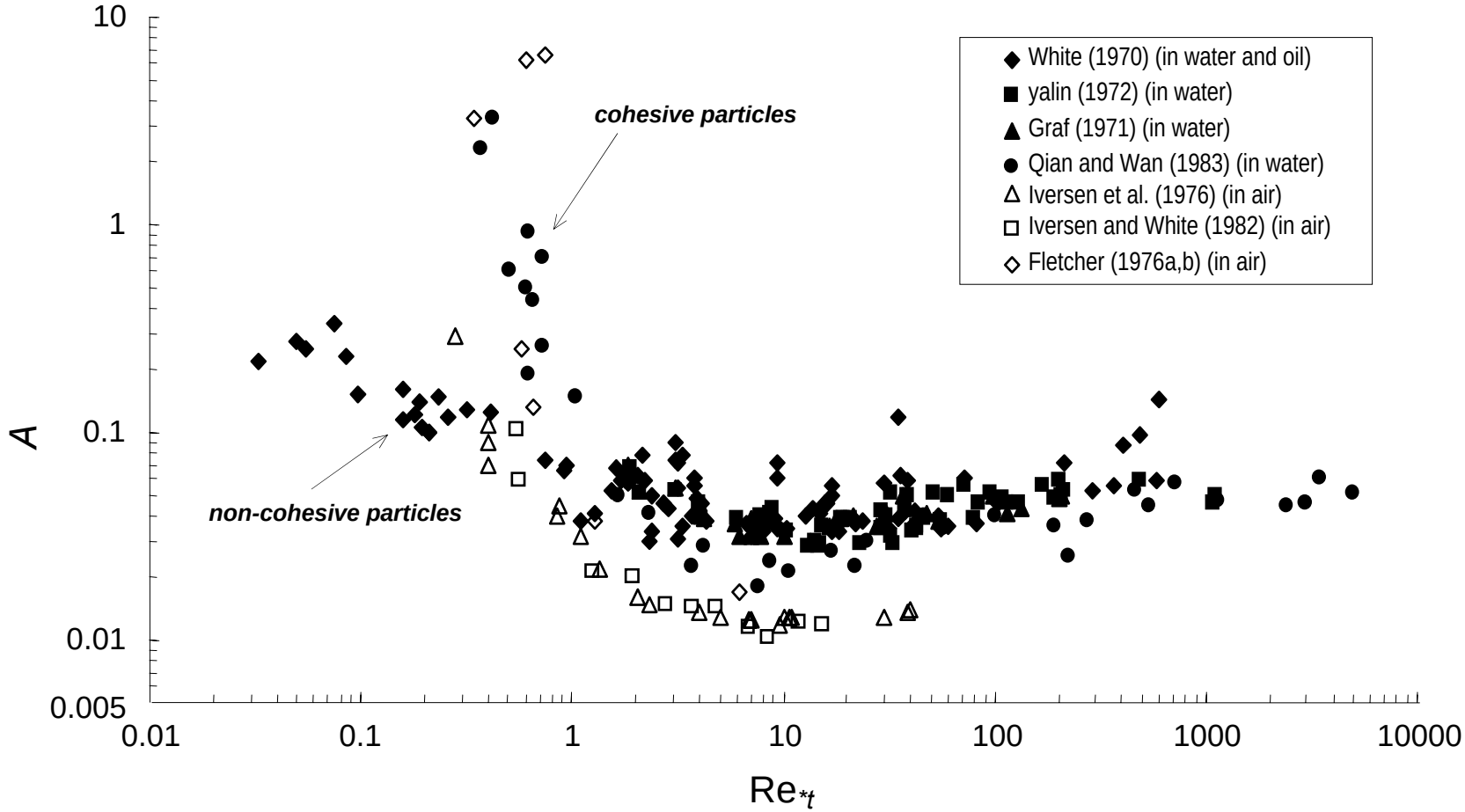
10
1
0.1
0.01
0.005
A
0.01
0.1
1
10
100
1000
10000
Re*t
cohesive particles
non-cohesive particles
White (1970) (in water and oil)
yalin (1972) (in water)
Graf (1971) (in water)
Qian and Wan (1983) (in water)
Iversen et al. (1976) (in air)
Iversen and White (1982) (in air)
Fletcher (1976a,b) (in air)

Figure 1

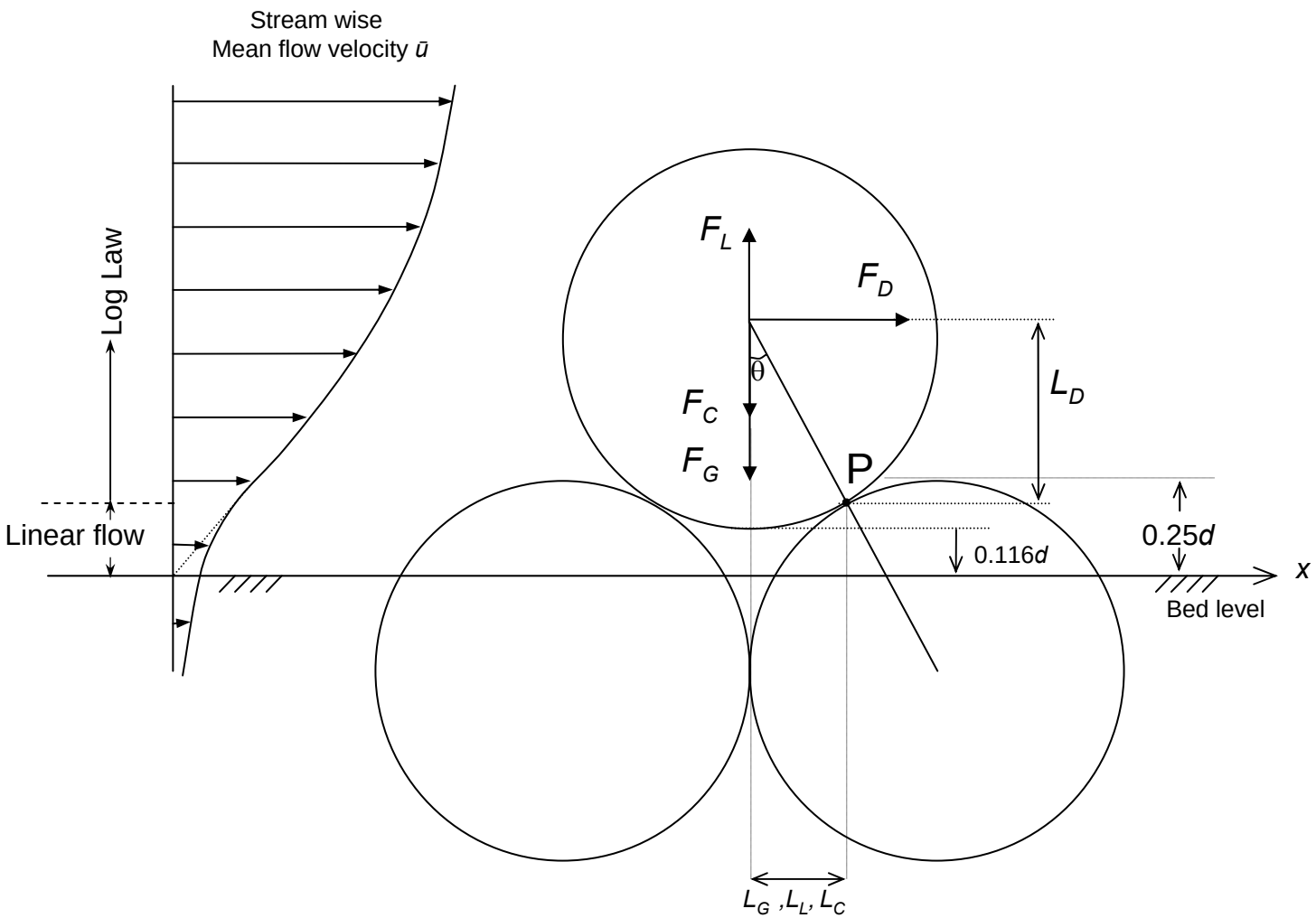
Stream wise
Mean flow velocity $\bar{u}$
Log Law
Linear flow
F_L
F_D
F_C
F_G
θ
P
L_D
0.116d
0.25d
Bed level
x
L_G ,L_L, L_C

Figure 2

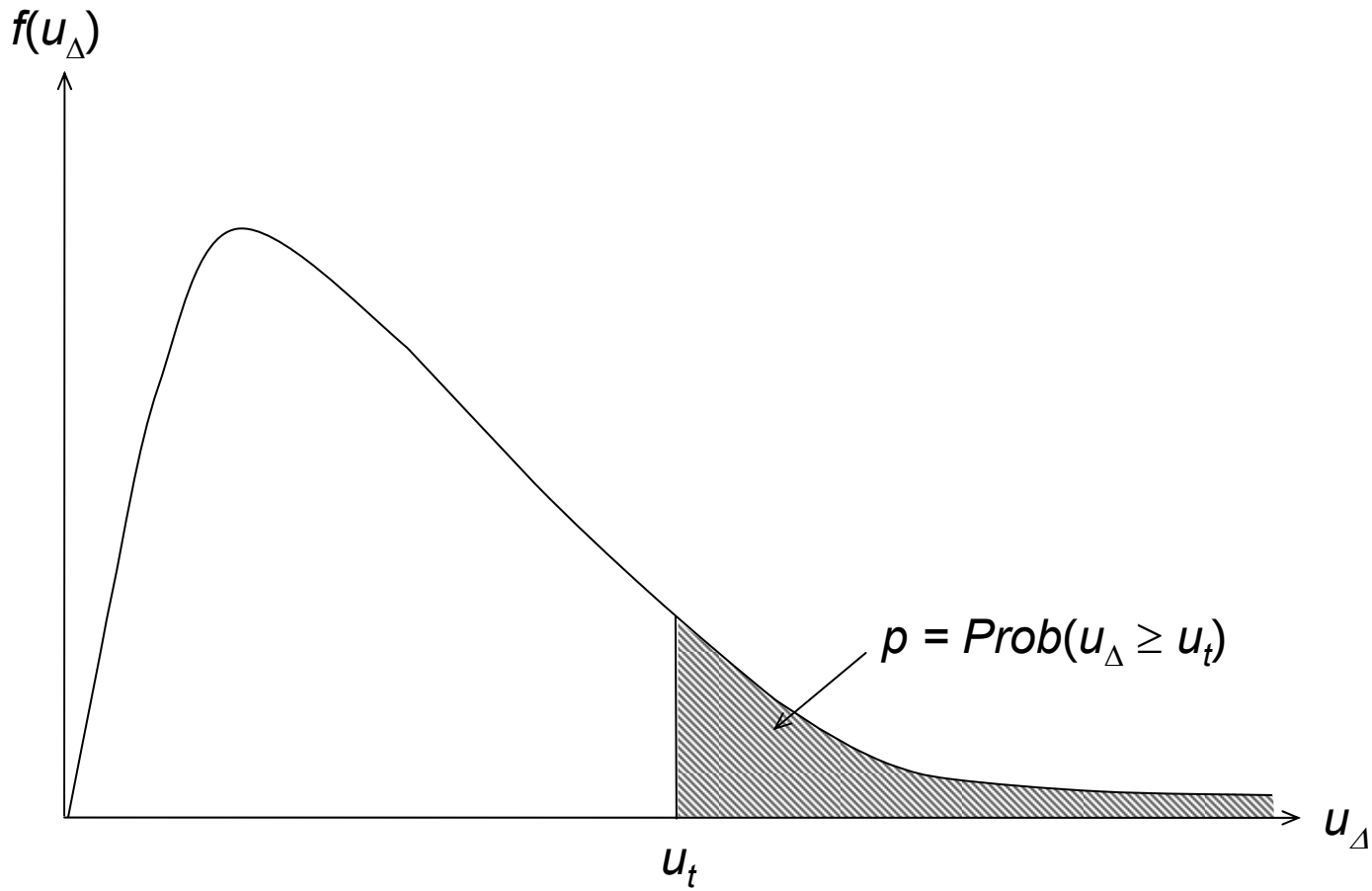

Figure 3

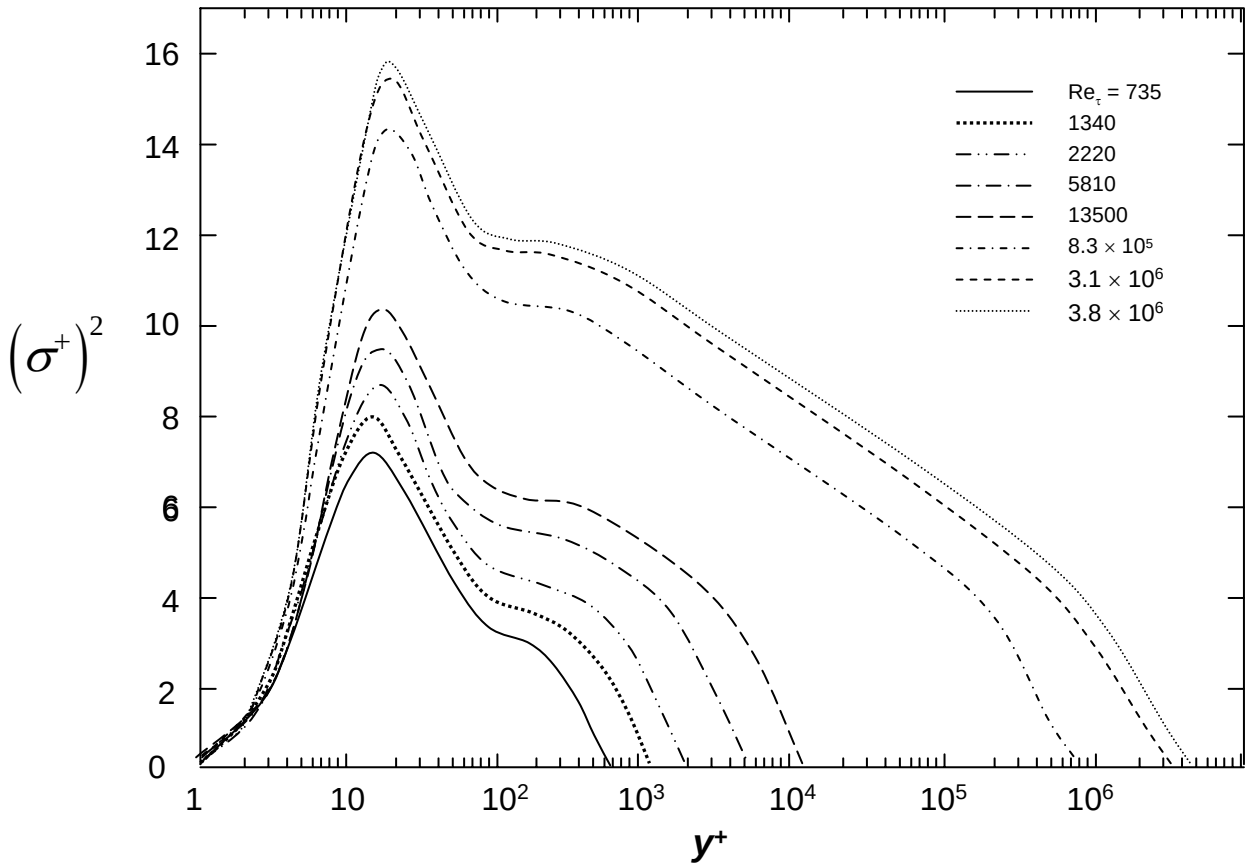
$\left(\sigma^+\right)^2$
16
14
12
10
8
6
4
2
0
1
10
10^2
10^3
10^4
10^5
10^6
y^+
Re_τ = 735
1340
2220
5810
13500
8.3×10^5
3.1×10^6
3.8×10^6

Figure 4

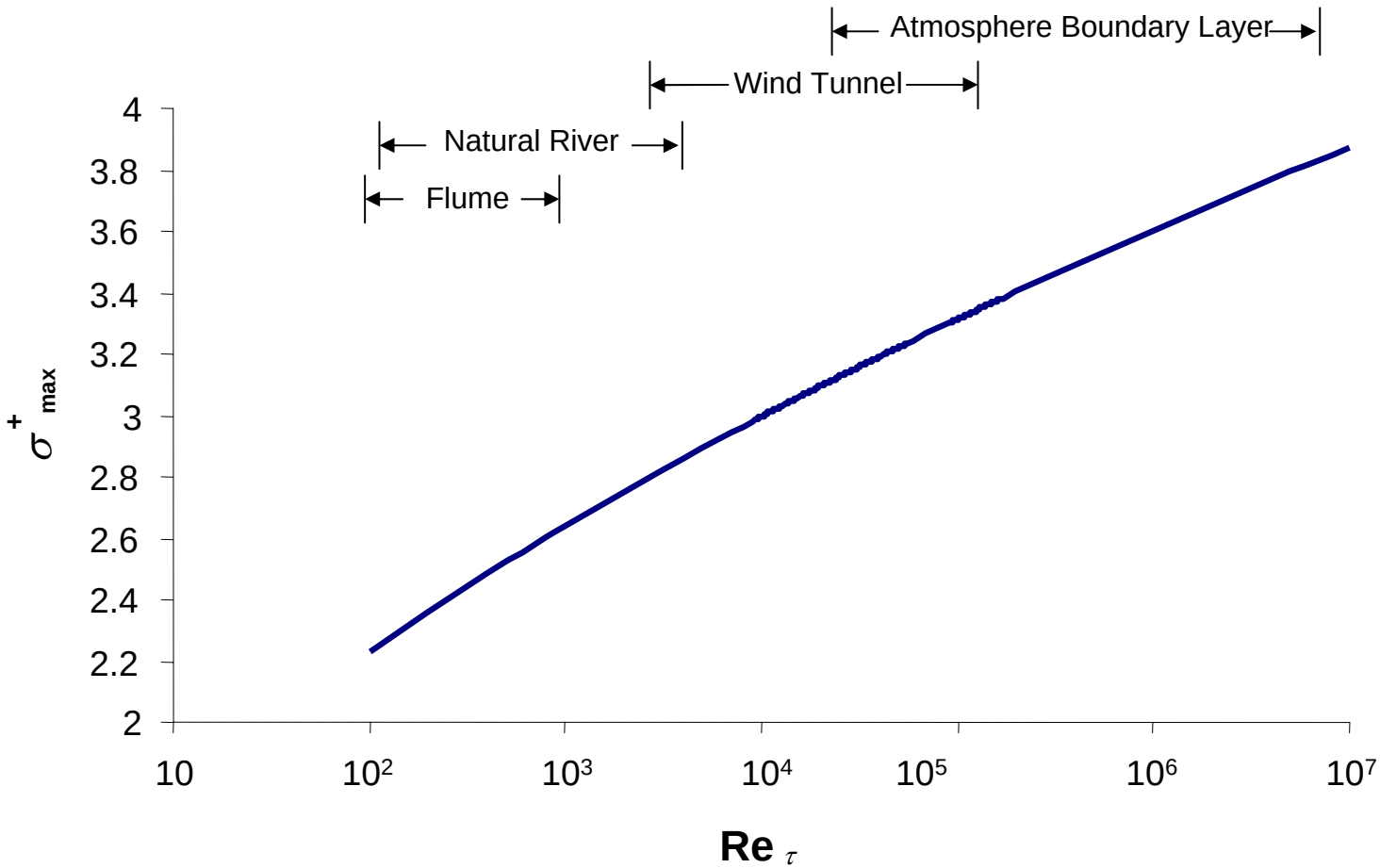
Atmosphere Boundary Layer
Wind Tunnel
Natural River
Flume
4
3.8
3.6
3.4
3.2
3
2.8
2.6
2.4
2.2
2
σ^+_{max}
10
10^2
10^3
10^4
10^5
10^6
10^7
Re_τ

Figure 5

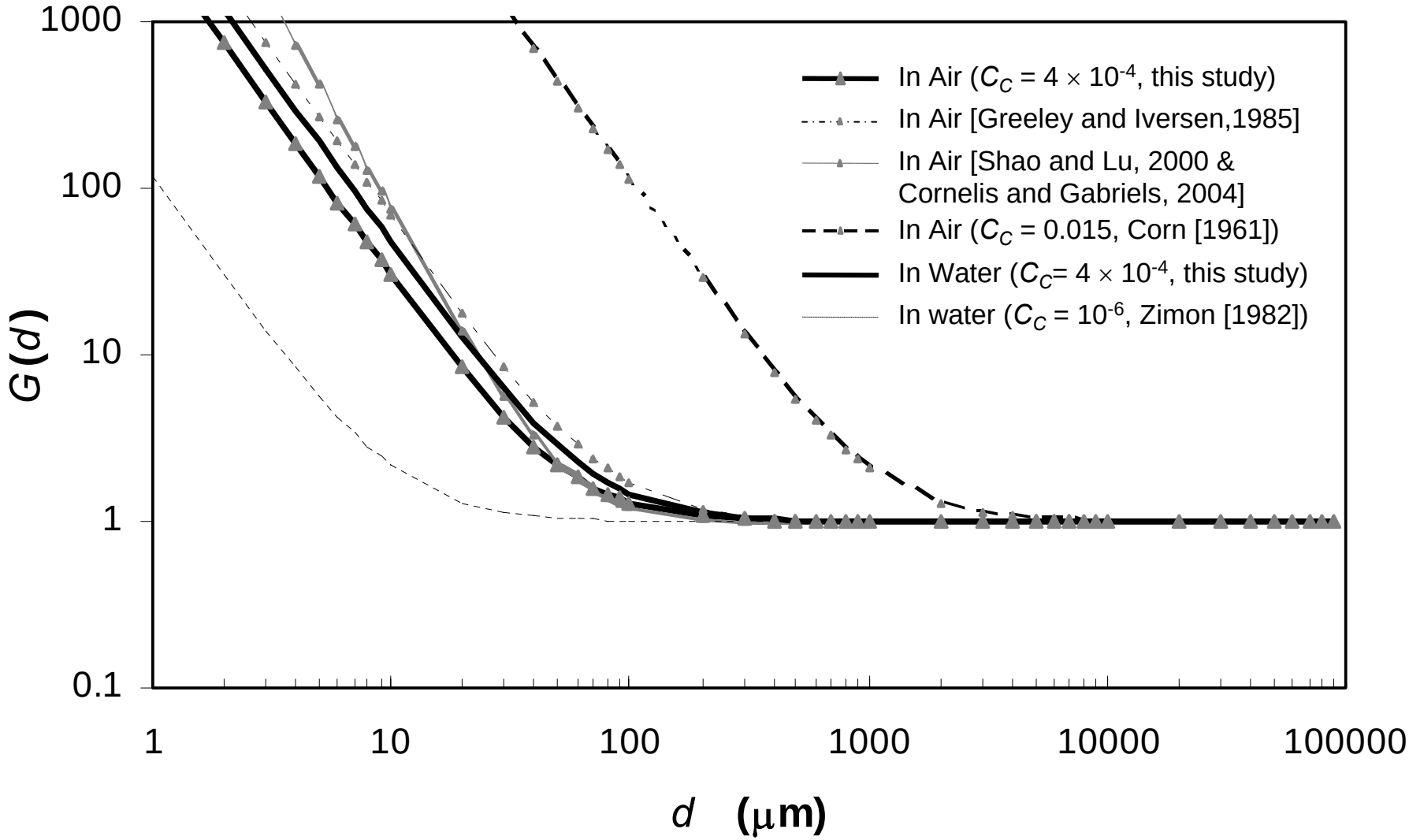
1000
100
10
1
0.1
G(d)
1
10
100
1000
10000
100000
d (μm)
In Air (C_C = 4 × 10^{-4}, this study)
In Air [Greeley and Iversen,1985]
In Air [Shao and Lu, 2000 & Cornelis and Gabriels, 2004]
In Air (C_C = 0.015, Corn [1961])
In Water (C_C= 4 × 10^{-4}, this study)
In water (C_C = 10^{-6}, Zimon [1982])

Figure 6

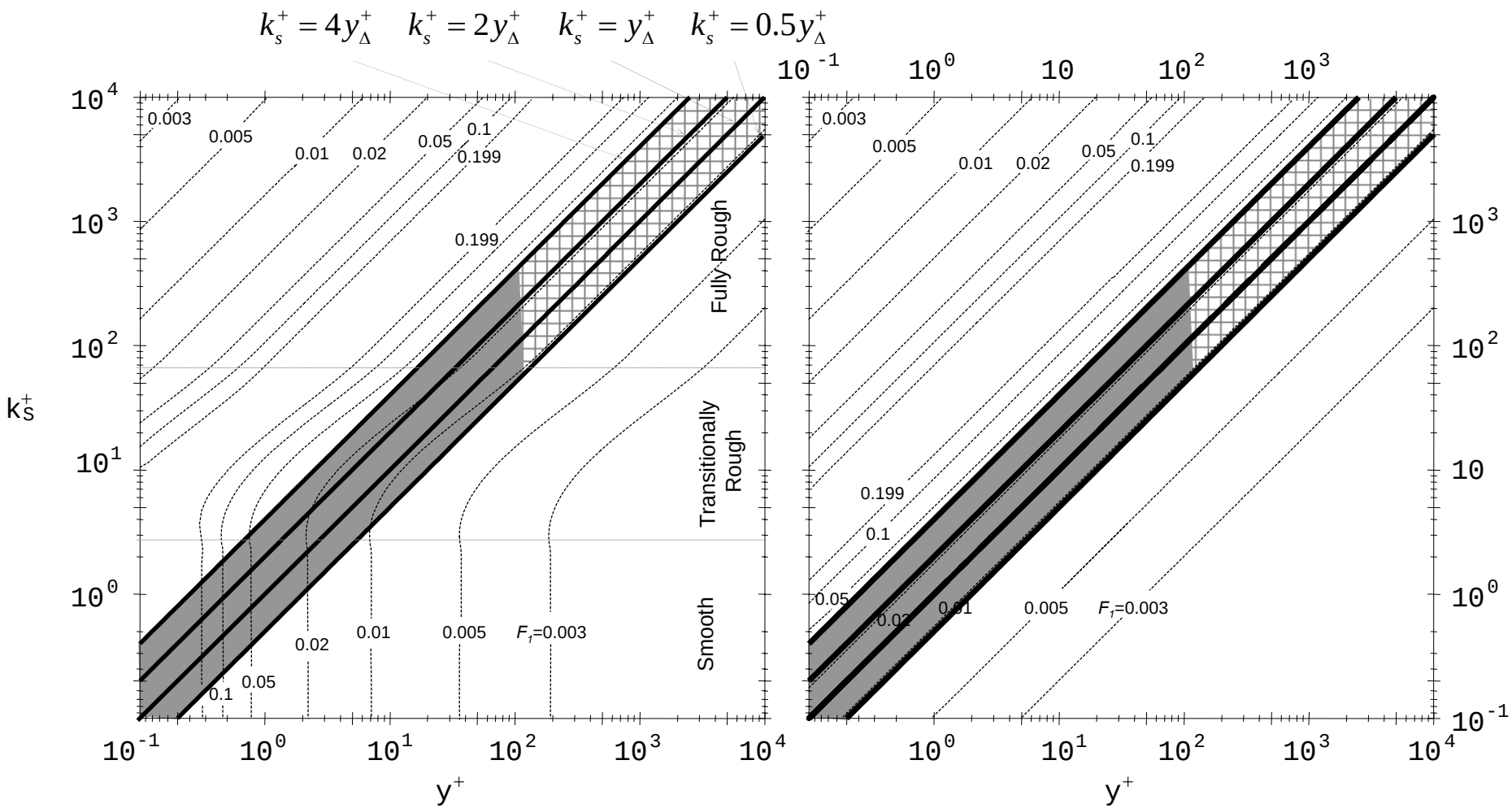
$k_s^+ = 4y_\Delta^+$
$k_s^+ = 2y_\Delta^+$
$k_s^+ = y_\Delta^+$
$k_s^+ = 0.5y_\Delta^+$
k_S^+
y^+
Fully Rough
Transitionally Rough
Smooth
F_1=0.003
(a)
(b)

Figure 7

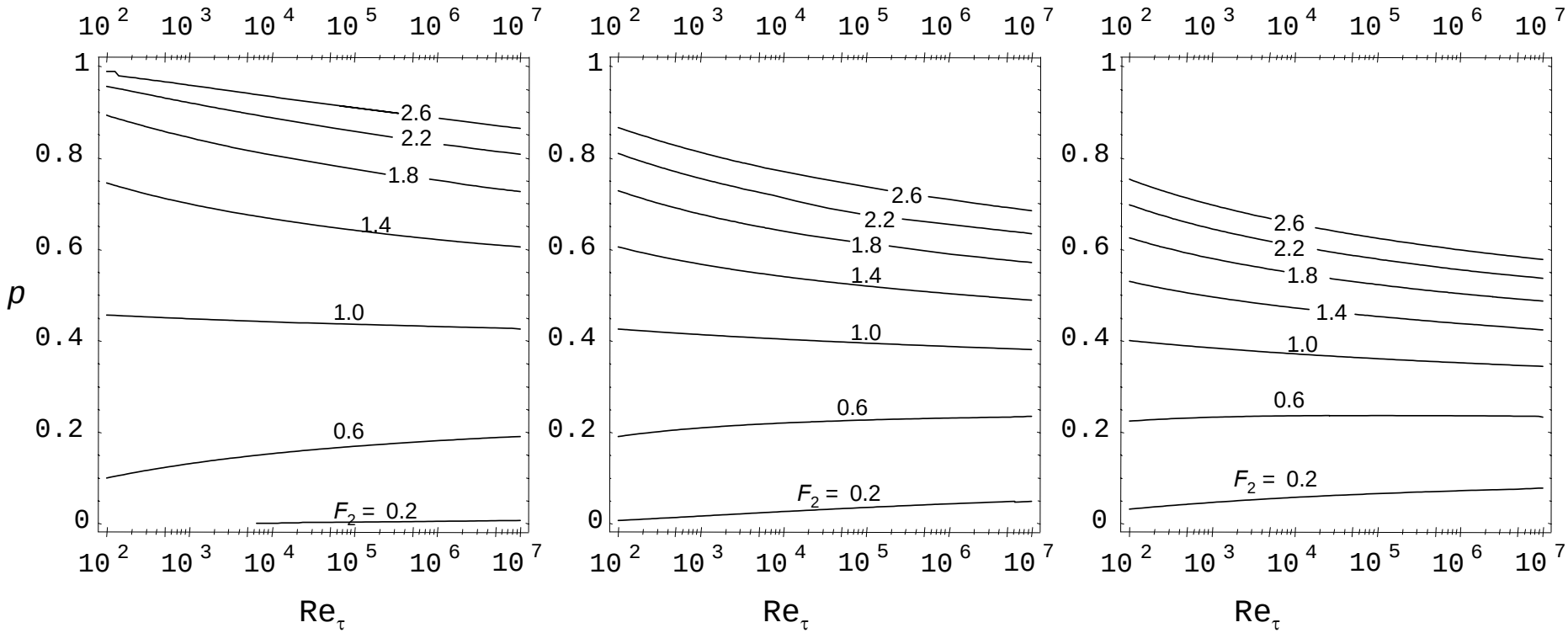

Figure 8

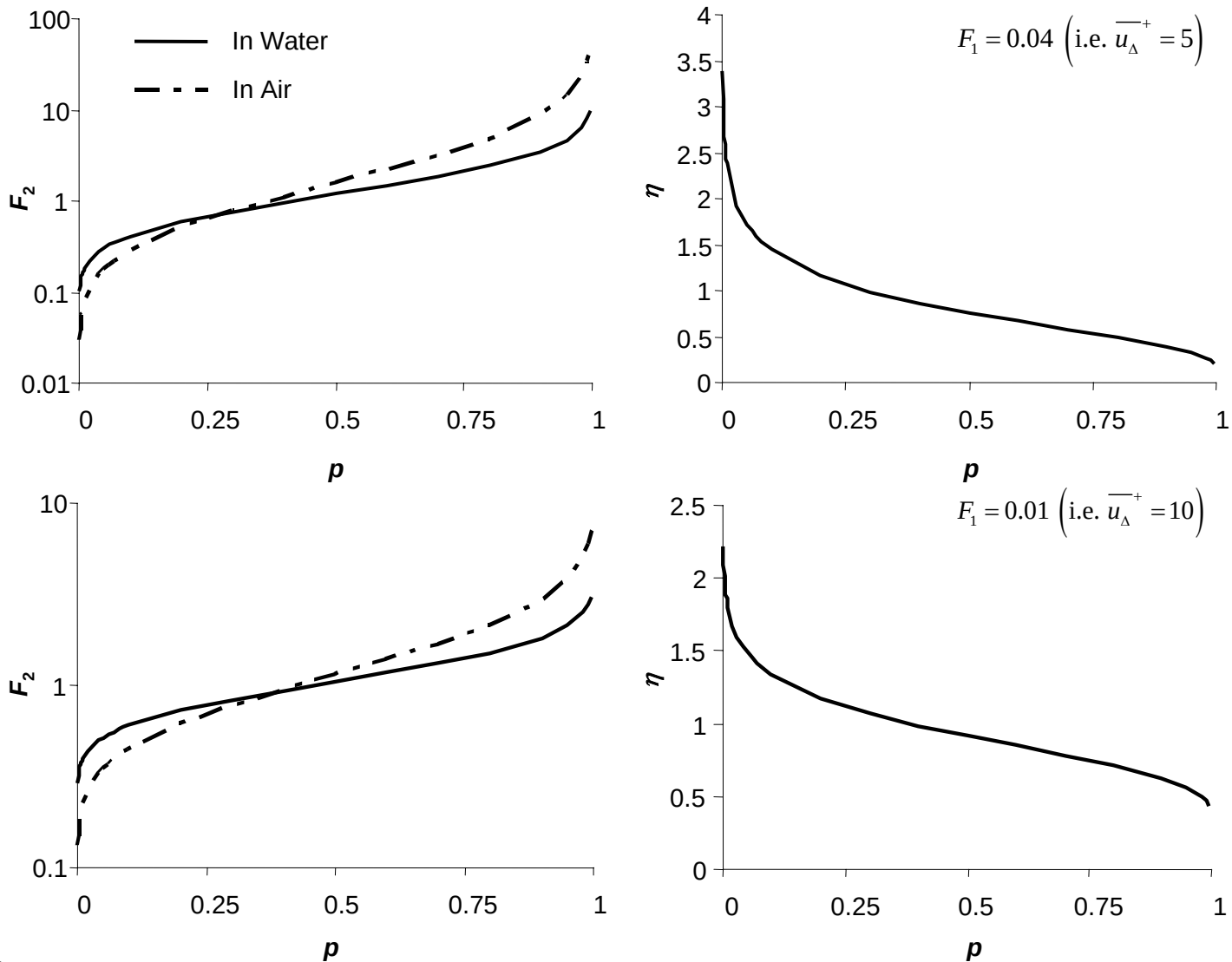
In Water
In Air
F_2
p
η
$F_1 = 0.04$ (i.e. $\overline{u_\Delta}^+ = 5$)
$F_1 = 0.01$ (i.e. $\overline{u_\Delta}^+ = 10$)

Figure 9

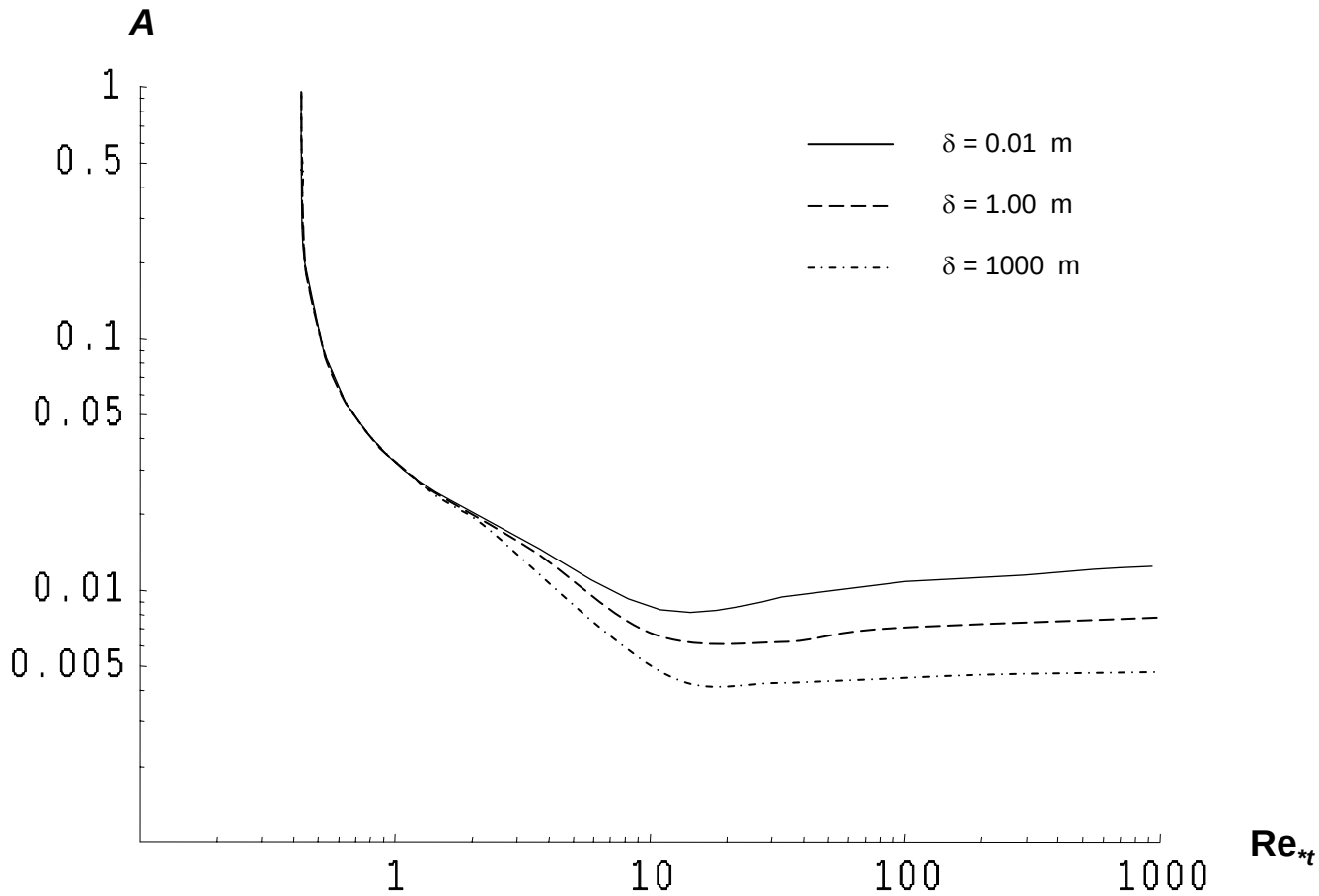

Figure 10

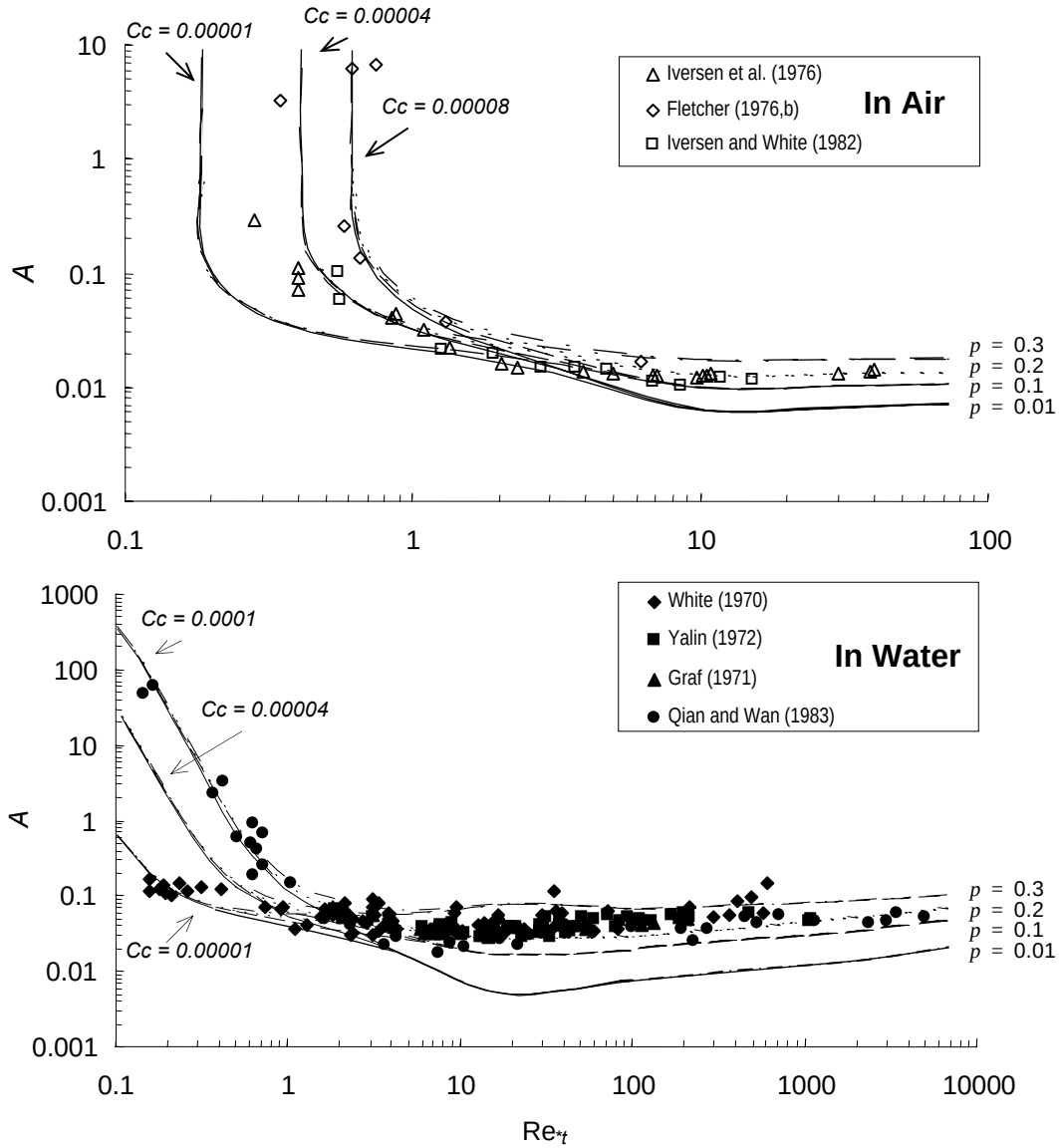
Cc = 0.00001
Cc = 0.00004
Cc = 0.00008
Iversen et al. (1976)
Fletcher (1976,b)
Iversen and White (1982)
In Air
p = 0.3
p = 0.2
p = 0.1
p = 0.01
A
10
1
0.1
0.01
0.001
0.1
1
10
100
Cc = 0.0001
Cc = 0.00004
Cc = 0.00001
White (1970)
Yalin (1972)
Graf (1971)
Qian and Wan (1983)
In Water
1000
100
10000
Re*t